Early Jurassic carbon-isotope perturbations in a shallow-water succession from the Tethys Himalaya, southern hemisphere

Zhong Han [1, 2], **Xiumian Hu** [2, *], **Marcelle BouDagher-Fadel** [3], **Hugh C. Jenkyns** [4] **Marco Franceschi** [5]

1 State Key Laboratory of Oil and Gas Reservoir Geology and Exploitation, Institute of Sedimentary Geology, Chengdu University of Technology, Chengdu 610059, China

2 State Key Laboratory of Mineral Deposit Research, School of Earth Sciences and Engineering, Nanjing University, Nanjing 210023, China

3 Department of Earth Sciences, University College London, London WC1H 0BT, UK

4 Department of Earth Sciences, University of Oxford, South Parks Road, Oxford OX1 3AN, UK

5 Department of Mathematics and Geosciences, Università degli Studi di Trieste, via Edoardo Weiss, 2, 34128, Trieste, Italy

*Corresponding author: Dr. Xiumian Hu

E-mail: huxm@nju.edu.cn; Tel: 0086 25 89683002

ABSTRACT

The Early Jurassic was characterized by extreme carbon-cycle perturbations that are associated with abrupt environmental and climatic change. However, the evidence mainly derives from sections in the western Tethys and northern Europe: localities situated in the northern hemisphere. This paper presents new records of foraminiferal biostratigraphic, sedimentological and carbonate carbon-isotope ($\delta^{13}C_{carb}$) data from the Tibetan Kioto Platform formed in the southeastern Tethys (southern hemisphere) during the Sinemurian–lowermost Toarcian interval. Six foraminiferal zones have been recognized: late Sinemurian *Textulariopsis sinemuriensis,* Pliensbachian *Planisepta compressa, Bosniella oenensis, Cyclorbitopsella tibetica* and *Streptocyclammina liasica,* and earliest Toarcian *Siphovalvulina* sp. A. Based on biostratigraphy, $\delta^{13}C_{carb}$ data allow correlation with coeval records from the western Tethys and northern Europe by the identification of both negative and positive $\delta^{13}C$ excursions. The negative excursions characterize the Sinemurian–Pliensbachian boundary event (SPBE) and the *margaritatus–spinatum* zone boundary event (MSBE); the positive $\delta^{13}C$ excursion characterizes the *margaritatus* zone event (ME). Facies evolution in the Early Jurassic indicates that the establishment of carbonate sedimentation on the Kioto Platform occurred in the context of a global sea-level rise partly coincident with the SPBE and that, in common with other coeval platforms, carbonate production following the negative shift was predominantly made up of skeletal carbonates. Furthermore, the spread of the *Lithiotis* Fauna on the Kioto Platform followed the rebound of isotopic values after the SPBE. This phenomenon has been observed in the Western Tethys and suggests that the global biocalcification event represented by the flourishing of the *Lithiotis* Fauna may have occurred synchronously across the Tethys, possibly reflecting the creation of more favourable marine conditions after the SPBE. Biostratigraphic data indicate that certain index larger benthic foraminifera became extinct around the onset level of the MSBE, likely due to the deleterious impact of this event. However, as in

more northerly localities, the *Lithiotis* Fauna persisted during the late Pliensbachian in the shallow-water platforms of the Tethys until its disappearance in the early Toarcian.

Keywords. Early Jurassic, carbonate platform, larger benthic foraminifera, carbon-isotope perturbations, *Lithiotis* Fauna, Tibetan Himalaya

1. Introduction

The Early Jurassic saw the rifting of the super-continent Pangaea with the separation of Africa from North America. During this period, important volcanic activity is indicated by the emplacement of the Central Atlantic Magmatic Province (CAMP) and Karoo-Ferrar Large Igneous Provinces (LIPs). The palaeontological and sedimentary records indicate that severe global environmental and climate changes occurred during this interval (e.g. Bond and Wignall, 2014). Two major environmental and biotic crises, characterized by the deposition of large volumes of organic-rich black shale in the oceans, took place around Triassic–Jurassic boundary time and early in the Toarcian stage (Toarcian oceanic anoxic event, T-OAE) and coincided with the activity of the CAMP and Karoo-Ferrar LIPs, respectively (e.g. Pálfy and Smith, 2000; Blackburn et al., 2013; Ruhl et al., 2020). The geochemical fingerprint of this subaerial volcanism is seen in the sedimentary mercury records from several continents (Percival et al., 2015, 2017).

Although considerable work has focused on these two events, the long-term environmental and climatic changes operating in the intervening period remain less well documented. An increasing number of studies have, however, led to recognition of other significant perturbations of the carbon-isotope record: the Sinemurian–Pliensbachian boundary event (SPBE), the *margaritatus* zone event (ME) mainly in the *margaritatus* zone, the *margaritatus–spinatum* zone boundary event (MSBE), and the Pliensbachian–Toarcian boundary event (PTBE). As documented in Europe and northern Africa, the SPBE, MSBE and PTBE are characterized by negative carbon-isotope excursions (CIE), whereas the ME is characterized by a positive excursion (e.g. Hesselbo et al., 2007; Littler et al., 2010; Korte and Hesselbo, 2011; Franceschi et al., 2014, 2019; Peti et al., 2017; Baghli et al., 2020). These and other features of the Lower Jurassic $\delta^{13}C$ curve are documented in great detail in the organic carbon-isotope records from the Sancerre-Couy borehole (France, Peti et al., 2017) and the Mochras Borehole (UK, Storm et al., 2020). Hitherto, it has been proposed that the SPBE environmental and climatic perturbations may have affected the microbially dominated carbonate platforms in the southern margins of the western Tethys and influenced the spread of the large thick-shelled bivalves of the *Lithiotis* Fauna (Franceschi et al., 2014, 2019) that became major reef builders in the Early Jurassic (Leinfelder et al., 2002; Fraser et al., 2004; Posenato and Masetti; 2012), but the possible wider influence of such processes has not been explored.

This study presents high-resolution carbonate carbon-isotope ($\delta^{13}C_{carb}$) data, foraminiferal biostratigraphy, and facies descriptions from the Sinemurian–lowermost Toarcian of the Wölong section, Tethys Himalaya, Tibet, which was located on the southeastern Tethyan margin, in the southern hemisphere at that time (Fig. 1). Biostratigraphic, isotopic and sedimentological data are used to propose a correlation between the eastern and western Tethys and to discuss how environmental changes may have influenced carbonate-platform evolution in the area.

2. Geological setting and stratigraphy

The study area is located in the Tethys Himalaya, Tibet, representing the northern margin of the Indian sub-continent (Fig. 1), bounded by the Yarlung Zangbo Suture Zone to the north and by the Greater Himalaya to the south. In the southern part of the Tethys Himalaya, a succession encompassing mixed shallow-water carbonates and siliciclastics is exposed, while the northern part exposes deep-water sediments (Liu and Einsele, 1994; Sciunnach and Garzanti, 2012). These successions were deposited during the Early Jurassic at low latitude (23.8°S [21.8°S, 26.1°S]) in the southern hemisphere on the mature passive margin of the southeastern Neotethys (Fig. 1A; Liu and Einsele, 1994; Jadoul et al., 1998; Sciunnach and Garzanti, 2012; Huang et al., 2015). The shallow-water carbonates of the Lower Jurassic in the Tethys Himalaya from Zanskar (India) to southern Tibet (China) are referred to as deposits of the Kioto Carbonate Platform (Gaetani and Garzanti, 1991; Jadoul et al., 1998; Sciunnach and Garzanti, 2012; Han et al., 2016, 2018).

The Wölong section, southern Tibet, China, is located in the southern part of the Tethys Himalaya (Fig. 1B; 28°29′2″N, 87°02′3″E). The studied sequence is ~219 m thick and comprises, from bottom to top, the Zhamure (~125 m), Pupuga (~92 m) and

Nieniexiongla (~2 m) formations. The Zhamure Formation is made up of mixed carbonate-siliciclastic deposits referred to a barrier-island and lagoonal environment (Han et al., 2016). This unit has been roughly ascribed to the Rhaetian(?)–lower Sinemurian based on benthic foraminifera found in the overlying Pupuga Formation and lithostratigraphic correlation (Jadoul et al., 1998; Han et al., 2016). The Pupuga Formation is characterized by a significant decrease in the siliciclastic component and by dominant bioclastic grainstones/packstones deposited on a shallow-water carbonate platform with moderately vigorous water circulation (Han et al., 2016). The larger benthic foraminifera *Orbitopsella praecursor* and large, aberrant bivalves belonging to the *Lithiotis* Fauna are found in the lower and upper part of this unit, respectively, indicating a Pliensbachian age (Jadoul et al., 1998; Wignall et al., 2006; Han et al., 2016).

The signature of the Toarcian ocean anoxic event (T-OAE) has been identified at the Pupuga–Nieniexiongla Formation boundary based on biostratigraphical, sedimentological, carbon- and sulphur-isotope data (Jadoul et al., 1998; Newton et al., 2011; Han et al., 2016, 2018). Consequently, the Pupuga Formation must encompass the lower Pliensbachian to lowest Toarcian interval. The Nieniexiongla Formation comprises outer-water ramp carbonates and is mainly composed of micrite alternating with coarser grained redeposited carbonate-rich layers interpreted as storm deposits. This formation is poorly dated as Toarcian–Aalenian in age (Han et al., 2018). Although Wignall et al. (2006) published preliminary research on the upper Pliensbachian-–lower Toarcian carbon isotopes in the Yunjia section of Tibet, ~500 m away from the Wölong

Commented [BM1]: As the word is plural so it is not capital letter

Commented [H2]: Is this OK? Are they skeletal grains?
Reply: “carbonate-rich” is ok. However, not all skeletal grains. These layers are usually dominated by peloid, ooid and skeletal grains, as well as quartzs.

section, the charactersitic events mentioned above were not identified due to relatively low-resolution $\delta^{13}C$ data and limited biostratigraphic control.

3. Material and methods

3.1 Foraminiferal biostratigraphic analysis

A total of 112 samples from the Wölong section were studied using the larger benthic foraminifera foraminifera (LBF). The LBF biozones in this study were compared with those from the characteristic carbonate platform in the western Tethys to determine age of the sedimentary succession. All the LBF were identified and the main species are plotted in Fig. 3, in relation to the new proposed foraminiferal biozonations.

Commented [H3]: Out of how many samples collected overall?
Reply: I think it does not make too much sense to state the total number. Additionally, we did not present it in 3.2 and 3.3

3.2 Point-counting in thin-section and facies analysis

A total of 176 samples of the Wölong section were used for quantitative estimates of abundance of terrigenous and skeletal carbonate grains (including common foraminifera, and fragments of bivalves, brachiopods, gastropods, sponges, echinoderms, etc.). These estimates were carried out through point-counting on thin-sections using the Image J software. Thin-section photographs were taken when the field-of-view best represented the petrological character of the sediment. For grainstone and packstone facies, the number of grains was usually more than 300 in the field-of-view. The grains in the photographs were circled using polygon or freehand selections and their area ratio was calculated automatically.

In the shallow-water carbonate-platform settings, the content and diversity of terrigenous and skeletal carbonate grains is sensitive to changes in sea level and environment (Flügel, 2010). Combined with the previous detailed results of microfacies analysis by Han et al. (2016), we use these newly obtained quantitative data on changes in relative abundance of quartz and skeletal carbonate grains through the section to establish a more detailed characterization of the evolution of the Kioto Carbonate Platform. In order to obtain a more comprehensive understanding of the entire evolution in Tethyan carbonate systems across the Early Jurassic, the facies data from this study and Han et al. (2016) were compared with those from the well-studied Trento Carbonate Platfrom, Italy of the western Tethys (Franceschi et al., 2014, 2019).

3.3 Carbon- and oxygen-isotope analysis

A total of 91 carbonate-rich samples from the Wölong section were selected for analysis of whole-rock carbonate carbon and oxygen isotopes. Cement-filled veins and pores, or larger bioclasts, were avoided during micro-drilling to obtain powders. Samples were dissolved by purified phosphoric acid (H_3PO_4) at 70°C and the evolved CO_2 was measured by a Finnigan MAT Delta Plus XP mass spectrometer coupled to an in-line GasBench II autosampler for isotope ratios at Nanjing University. Results are reported in the standard delta notation in per mil deviation from the Vienna Pee Dee Belemnite (VPDB) standard. Replicated measurements of a standard show an analytical precision (1σ error) of 0.05‰ for $\delta^{13}C_{carb}$ and 0.07‰ for $\delta^{18}O_{carb}$.

4. Results

4.1. Biostratigraphy

The studied samples are moderately fossiliferous and the ubiquitous presence of LBF has enabled production of a high-resolution biostratigraphy based on these organisms (Fig. 2).

In the past, the Lower Jurassic inner platform carbonates have proved difficult to date. Data presented in this paper enable stage and sub-stage level dating through biostratigraphic comparison with Western Tethyan biozones (BouDagher-Fadel and Bosence, 2007). From this regional biostratigraphic study, it is clear that six biozones can be recognized. The LBF distribution is plotted in order to understand the chronostratigraphy and the depositional palaeoenvironments of the Early Jurassic in the Tethys Himalaya, thereby producing a new pan-Tethyan LBF biozonation scheme. Most index fossils described below are shown in Fig. 3. The LBF as a whole are comparable to those described from the inner carbonate platform environments widespread along the rifted western margins of the Early Jurassic Tethys, notably those recorded from Morocco, Italy and Greece as well as southern Spain (see detailed results below, cf. Barattolo and Romano, 2005; BouDagher-Fadel and Bosence, 2007; BouDagher-Fadel, 2018).

Textulariopsis sinemuriensis zone (≈ *raricostatum* ammonite zone): This zone is equivalent to the western Tethyan Zone of *Lituosepta recoarensis* and *Orbitopsella* spp. zone (Fig. 4) and corresponds to the upper Sinemurian (~18–60 m). The foraminifera of this zone are rare and recrystallized and are mainly small textularids and *Siphovalvulina* spp. Assemblages include *Siphovalvulina colomi* (Fig. 3A), *S. gibraltarensis, Duotaxis metula*, *Textulariopsis sinemurensis* and *Cyclorbitopsella* sp. The presence of *Siphovalvulina colomi* and *Textulariopsis sinemurensis* indicates a Sinemurian–early Pliensbachian age (BouDagher-Fadel et al., 2001; Noujaim Clark and BouDagher-Fadel, 2004; BouDagher-Fadel and Bosence, 2007; Gale et al., 2018), but the occurrence of *Cyclorbitopsella* sp. at 33.3 m points to an age not older than late Sinemurian (BouDagher-Fadel and Bosence, 2007; BouDagher-Fadel, 2018). The absence of species such as *Orbitopsella primaeva, Lituosepta recoarensis* and *Everticyclammina praeviguliana*, which first appear in the upper Sinemurian of the western Tethyan province, is notable and most likely due to the poor preservation of the microfauna at this horizon.

Planisepta compressa zone (≈ *jamesoni* ammonite zone) (Fig. 4): This zone is characterized by the presence of *Planisepta compressa* and *Rectocyclammina* species, which indicates the onset level of the Pliensbachian stage (~60–125 m). It also includes *Siphovalvulina colomi, Everticyclammina praevirguliana* (Fig. 3C), *Orbitopsella primaeva*, *Textularia* sp., *Lituosepta recoarensis* Cati (Fig. 3D), *Mesoendothyra* sp., *Glomospira* sp., *Siphovalvulina gibraltarensis*; and dasyclad spp. are common. Foraminifera of this subzone are well preserved, which explains the appearance of many upper Sinemurian species that are not preserved in the stratigraphically underlying horizon.

Bosniella oenensis zone (≈ *ibex* ammonite zone) (Fig. 4): *Bosniella oenensis* (Fig. 3E) is common throughout the upper Sinemurian and lower Pliensbachian of the western Tethyan region (BouDagher-Fadel, 2018) but first appears in Tibet at this horizon indicating the uppermost part of the lower Pliensbachian stage (~125–132 m). *Cyclorbitopsella tibetica* and *Orbitopsella praecursor* are also still common over this interval.

Cyclorbitopsella tibetica zone (≈ *davoei* ammonite zone) (Fig. 4): This zone is represented by the disappearance of *Bosniella oenensis* and corresponds to the lowest part of the upper Pliensbachian (~132–153 m). This zone is characterized by the common occurrences of *Cyclorbitopsella tibetica*. Other upper Sinemurian–Pliensbachian forms such as *Orbitopsella primaeva* (Fig. 3G), *Orbitopsella praecursor* (Fig. 3H), *Mesoendothyra* sp., *Streptocyclammina liasica, Lituosepta recoarensis* and *Planisepta compressa* (Hottinger) (Fig. 3I) are still present.

Streptocyclammina liasica zone (≈ *margaritatus and spinatum* ammonite zones) (Fig. 4): This zone corresponds to the upper Pliensbachian (~153–208 m). *Streptocyclammina liasica*, which ranges from Pliensbachian to Toarcian in the western Tethyan province (BouDagher-Fadel, 2018), makes its first appearance in this zone. LBF include *Pseudocyclammina* sp., *Streptocyclammina liasica* (Fig. 3J), *Lituosepta recoarensis*, *Siphovalvulina* sp., *Glomospira* sp., *Mesoendothyra* sp., *Siphovalvulina colomi*; small miliolids and fragments of algae are common throughout. Foraminifera are generally rare in the uppermost part of this zone. They include *Palaeomayncina termieri* (Fig. 3K), *Haurania* sp. A, *Planisepta compressa, Lituosepta recoarensis, Siphovalvulina* spp., *Glomospira* sp., *Siphovalvulina colomi*; small miliolids, and dasyclad sp. fragments occur commonly throughout this interval.

Siphovalvulina sp. A zone (≈ *tenuicostatum* ammonite zone) (Fig. 4). This zone corresponds to the lower Toarcian (~208–250 m) and to the western Tethyan *Socotraina serpentina* zone (see BouDagher-Fadel, 2018). Foraminifera in this zone are badly preserved and rare specimens of *Socrotaina* cf. *serpentina* are present only at one horizon of this interval. This zone is characterized by the appearance of *Siphovalvulina*

Commented [H4]: Is this correct? Check with Marcelle I have added a space. What does 'A' stand for?

Commented [BM5R4]: Yes Hugh this is right. It is a new species of Haurania but we do not have enough specimens to name it as new species sp we call it sp. A in order to differentiate from other Hauranias..

sp. A. (Fig. 3L) and the disappearance of *Planisepta compressa* (see BouDagher-Fadel, 2018). *Lituosepta recoarensis*, which ranges in the Western Tethys from upper Sinemurian to lower Toarcian, still persists in this zone. Other LBF include *Glomospira* spp., *Pseudopfenderina* sp., *Textularia* sp., *Mesoendothyra* cf. *croatica* (Fig. 3M), *Rectocyclammina* sp.; dasyclad spp. are also present.

Commented [H6]: Is this correct? I have added a space. Check with Marcelle.

Commented [BM7R6]: Yes it is right

4.2. Sedimentological observations

The Lower Jurassic of the Wölong section is characterized by mixed carbonate–siliciclastic facies in the lower part and by mainly carbonate facies in the upper part. Overall, therefore, the terrigenous and carbonate content decreases and increases from bottom to top, respectively (Fig. 9). Terrigenous material is dominated by quartz grains (mainly ranging from 0.1 to 0.2 mm in diameter) that are abundant in the bottom part of the section (~0–50 m), with a percentage typically varying from ~20% to ~90%, whereas skeletal carbonate grains vary in abundance from 0% to 10% (~2% on average; Fig. 9). Over the interval of the stratigraphically lowest negative CIE (~54–130 m), quartz and skeletal carbonate grains show an overall decrease and increase, respectively, compared to subjacent strata. In the overlying interval, quartz is significantly lower in abundance, with a content typically lower than 10% (~130–170 m), with sporadic occurrences of sandstones, but falls almost to zero over the interval ~170–220 m. By contrast, the skeletal carbonate grains content increases in the interval of ~130–220 m, with an average abundance of ~14% and peaks over 20% and 40% (Fig. 9).

4.3. Carbon and oxygen isotopes

$^{13}C_{carb}$ and $\delta^{18}O_{carb}$ data from the Wölong section mainly range from −1.5‰ to +2.5‰ and −6‰ to −15‰, with an average of 1‰ and −9‰, respectively (Fig. 5). $^{13}C_{carb}$ data present a broad overarching negative excursion (~54–130 m) with a magnitude of ~2.5‰; higher in the section values remain relatively constant between 1‰ and 1.5‰ (~130–146 m). Stratigraphically higher still, a positive CIE (~146–172 m) occurs that is immediately followed up-section by a second negative CIE (~172–202 m): both excursions have a magnitude of ~2‰ (Fig. 5). All data are provided in the Supplementary material.

5. Discussion

5.1. Influence of diagenesis and facies-dependency on $\delta^{13}C_{carb}$ from Wölong section.

Samples from Wölong display weak correlation between $\delta^{13}C_{carb}$ and $\delta^{18}O_{carb}$ (R^2 = 0.4558) (Fig. 6A). Although such a pattern can be suggestive of limited post-depositional change, covariance between $\delta^{13}C_{carb}$ and $\delta^{18}O_{carb}$ is not necessarily a fingerprint of diagenesis (Marshall, 1992; Swart and Oehlert, 2018): coincident changes in sea-surface temperature and global carbon cycling could, for example, produce such an effect. The overwhelming majority of $\delta^{18}O$ values in this study are less than ~−5‰, which are considered to be indicative of diagenetic alteration (cf. Kaufman and Knoll, 1995); such values are considerably more negative than expected for Early Jurassic seawater and are found at Wölong between ~21–130 m. Nevertheless, $\delta^{13}C_{carb}$ values in the same interval fall in the range ~−1‰ to 1.5‰, which is close to that (~−1‰ to

3‰) reported for skeletal calcite and bulk carbonate from coeval pelagic, epicontinental and platform-carbonate successions in European areas (cf. Jenkyns and Clayton, 1986, 1997; Dera et al., 2011; Korte and Hesselbo, 2011; Franceschi et al., 2014, 2019). These observations suggest that the $\delta^{18}O_{carb}$ values from the Wölong section underwent obvious diagenetic modification, while $\delta^{13}C_{carb}$ was relatively well preserved and more faithfully reflects the isotopic ratio of the Early Jurassic seawater. In general, carbon isotopes behave more conservatively than oxygen isotopes during diagenesis because the volume of carbon in any carbonate rock is vastly greater than in any potential reactive fluid and, unlike oxygen isotopes, recrystallization during burial at elevated temperature has only minor effect (e.g. Scholle and Arthur, 1980).

The samples used for $^{13}C_{carb}$ analysis are dominated by carbonates as mentioned above. The previous work shows that dolomite, micrite, wackestone, packstone, grainstone and sandy carbonate are dominant in the studied interval (Han et al., 2016) and therefore five characteristic facies were divided based on grain type and/or texture (Fig. 5C). Given that lithology may influence $\delta^{13}C_{carb}$, the characteristic facies of analysed samples were plotted against $\delta^{13}C_{carb}$ values (Fig. 5A). Each facies displays a wide range of $\delta^{13}C_{carb}$ values. Additionally, the box-plots show that the carbon-isotope values of each facies are close, mostly ranging from ~−1‰ to 1.5‰ (Fig. 6B). These observations therefore suggest that $\delta^{13}C_{carb}$ are not facies-dependent and that they likely reflect original seawater composition.

Detailed microfacies analysis shows that the studied interval was dominated by barrier-island, lagoonal and inner and open-platfrom environments (Han et al., 2016).

Due to the barrier island usually depositing quartz-rich sandstone, unsuitable for carbon-isotope analysis, the majority of samples for $\delta^{13}C_{carb}$ analysis are from two depositional environments, namely lagoon and inner and open platform, and the boundary is around the Zhamure–Pupuga contact. However, every major change in $\delta^{13}C_{carb}$ is recorded in sediments derived from a constant depositional environment, not across lithological transitions. In summary, local depositional environment and facies likely had a negligible influence on $\delta^{13}C_{carb}$.

5.2. The Sinemurian–Pliensbachian boundary event

A negative CIE at the Sinemurian–Pliensbachian boundary (SPBE) was first described from sections in the UK based on skeletal calcite from belemnites and brachiopods (Jenkyns et al., 2002; Korte and Hesselbo, 2011). Although Danisch et al. (2019) suggested that the SPBE CIE may respresent just a phase in which isotopic values return to previous values after a positive excursion during the late Sinemurian, several lines of evidence suggest that this negative CIE must be a genuine event. Evidence of the same CIE was widely reported in other sections from the western Tethys, including Portugal (Duarte et al., 2014), UK (Jenkyns et al., 2002; Korte and Hesselbo, 2011; Price et al., 2016; Storm et al., 2020), France (Peti et al., 2017), Italy (Woodfine et al., 2008; Franceschi et al., 2014, 2019), and Algeria (Baghli et al., 2020). The wide geographical expression of this CIE suggests that the phenomenon responsible for the perturbation in the carbon cycle had supra-regional impact. Furthermore, the CIE is recorded in carbonate, organic matter and fragments of terrestrial wood (e.g. Korte and Hesselbo, 2011; Peti et al., 2017; Franceschi et al., 2019), and therefore must reflect a perturbation of the carbon cycle that involved the whole ocean–atmosphere system. A correlation with demise of some western Tethyan carbonate platforms has been proposed, suggesting significant environmental change (Jenkyns, 2020).

Biostratigraphic data from the Wölong section allow the Zhamure Formation (~0–114 m) to be referred to the upper Sinemurian to lower Pliensbachian (Fig. 2). Although the foraminifera in the upper Sinemurian interval are rare and badly preserved, the lowest appearance of *Rectocyclammina* sp. can be taken to mark the boundary between the *Siphovalvulina colomi* zone and the *Lituosepta recoarensis* zone, as defined by Boudagher-Fadel (2018), and therefore identify the base of the Pliensbachian. With this constraint, the 2‰ negative CIE in $\delta^{13}C_{carb}$ starting at ~54 m can be correlated with the SPBE (Fig. 7), whose onset has been dated to the upper Sinemurian (*raricostatum* ammonite zone) and extends to the *davoei* ammonite zone in the middle portion of the Pliensbachian (cf. Storm et al., 2020). This correlation is strengthened by the features of the CIE at Wölong. Its magnitude is comparable to that of the SPBE in European successions and, furthermore, the shift is preceded by an interval in which isotopic values are roughly constant. This pattern is clearly visible in several $\delta^{13}C$ records from northern Europe and western Tethys (e.g. Korte and Hesselbo, 2011; Peti et al., 2017; Franceschi et al., 2019; Storm et al., 2020). The recognition of the SPBE in the southern hemisphere reinforces evidence that this CIE has global expression and therefore reflects a global-scale variation in the isotopic composition of the ocean-atmosphere reservoirs of the exogenic carbon cycle.

Based on current evidence, the SPBE is an isotopically negative carbon-cycle perturbation with a magnitude of ~2–4‰ in $\delta^{13}C_{carb}$ and ~5–7‰ in $\delta^{13}C_{org}$, respectively (Figs. 5 and 7). For the origin of the SPBE CIE, hypotheses such as enhanced hydrothermal activity in the context of Pangaean rifting (Franceschi et al., 2014, 2019) or late pulses of the Central Atlantic Magmatic Province (Ruhl et al., 2016; Shöllhorn et al., 2020) have been proposed, but the causal mechanism(s) of the negative excursion still remain unclear. Massive input of isotopically light carbon into ocean–atmosphere system would be expected to trigger global warming and ocean acidification. A negative excursion in $\delta^{18}O$ has been highlighted in lower Pliensbachian successions of western Tethys and northern Europe in coincidence with the main CIE of the SPBE (e.g. Dera et al., 2011; Baghli et al., 2020), which is suggestive of a warming phase. However, some authors have reported evidence of cooling in the latest Sinemurian/early Pliensbachian (Price et al., 2016; Korte and Hesselbo, 2011). This apparent discrepancy might suggest either that cooling was local or that a more complex evolution of climate was associated with the SPBE. Ocean acidification remains a possibility and may be implicated in the crisis/demise of some western Tethyan carbonate platforms (Franceschi et al., 2019; Jenkyns, 2020).

5.3 The late Pliensbachian–early Toarcian (pre-T-OAE) events

The features of the $\delta^{13}C_{carb}$ curve stratigraphically above the SPBE level in the Wölong section correspond well with the $\delta^{13}C_{carb}$ and $\delta^{13}C_{TOC}$ curves generated from the nearby Yunjia section that can be phisically correlated to Wölong (Fig. 5; cf Wignall et al., 2006). The Wölong and Yunjia records can therefore be combined to create the denser composite curve shown in Fig. 7. A positive shift with a magnitude of ~2‰ in $\delta^{13}C_{carb}$ (Wölong and Yunjia) and of ~4–5‰ in $\delta^{13}C_{TOC}$ (Yunjia) is observed (~146–172 m) in the lower Pupuga Formation (Fig. 7). Biostratigraphic constraints allow referral of this positive shift to the upper Pliensbachian (*S. liasica* LBF zone, roughly coincident with the *margaritatus* and *spinatum* ammonite zones) (Figs. 4 and 7). This feature correlates with a positive shift in the $\delta^{13}C$ record identified in the *margaritatus* ammonite zone in terrestrial and marine organic matter, wood and carbonate in European and North American successions (e.g. van de Schootbrugge et al., 2005; Suan et al., 2010; Korte and Hesselbo, 2011; Silva et al., 2011; Silva and Duarte, 2015; Ruhl et al., 2016; Peti et al., 2017; De Lena et al., 2019; Storm et al., 2020). This positive shift is named the margaritatus zone event (ME) following Korte and Hesselbo (2011), Ruhl et al. (2016) and De Lena et al. (2019). It is worth noting that the onset level of the ME in Wölong and Yunjia extends downward to the upper *Cyclorbitopsella tibetica* LBF zone, notionally correlative with the *davoei* ammonite zone (Figs. 4 and 5). This stratigraphic arrangement may suggest an earlier onset of the ME in the eastern Tethys than the western Tethys or, more probably, an apparent diachroneity due to lower resolution of the LBF scheme as compared to the ammonite biozonation.

The ME positive excursion has been attributed to burial of $\delta^{13}C$-depleted organic-rich sediment, which could be illustrated by the coeval widespread occurrence of black shales in Spain, Portugal and North America over this interval (Rosales et al., 2006;

Suan et al., 2010; Silva and Duarte, 2015; De Lena et al., 2019). This process could have drawn down CO_2 levels that had increased during the SPBE and thereby caused a cooling phase, as suggested by a coincident positive shift in $\delta^{18}O$ values in carbonate archives from a number of sections (e.g. Rosales et al., 2004; Suan et al., 2010; Korte and Hesselbo, 2011; Harazim et al., 2013; Korte et al., 2015; Baghli et al., 2020).

After the increase observed over the ME interval, $\delta^{13}C$ values undergo another negative excursion with a magnitude of ~2‰ in $\delta^{13}C_{carb}$ (Wölong and Yunjia) and of ~4‰ in $\delta^{13}C_{TOC}$ (Yunjia) in the upper Pupuga Formation (Fig. 5). This CIE occurs in the upper *Streptocyclammina liasica* LBF zone, equivalent approximately to the upper *margaritatus* and lower *spinatum* ammonite zones (Figs. 4 and 5) and, in the Wölong and Yunjia sections, closely follows the ME with a magnitude of ~2‰ in $\delta^{13}C_{carb}$ and ~4‰ in $\delta^{13}C_{TOC}$. This negative shift is here correlated with the *margaritatus–spinatum* boundary event (MSBE) that has been documented in carbonates, organic matter and wood fragments in multiple sections from European shelf seas and western Tethyan basins between the *margaritatus* and *spinatum* ammonite zones (Fig. 7; Korte and Hesselbo, 2011; Peti et al., 2017; Storm et al., 2020; Mercuzot et al., 2020). Based on these observations, the *spinatum–margaritatus* ammonite zone boundary in this study is positioned at the minimum $\delta^{13}C_{carb}$ value of this event (~200 m; Fig. 7). During the MSBE interval, a positive $\delta^{18}O$ excursion in skeletal calcite from the western Tethys and Arctic shelf areas has been reported, which suggests a cooling phase and possible regional sea-level fall (Rosales et al., 2006; Suan et al., 2010, 2011; Korte and Hesselbo, 2011; Korte et al., 2015). Therefore, this negative $\delta^{13}C$ excursion has been linked to release of isotopically light carbon from sediment reworking, organic-matter oxidation, and heterotrophic remobilization probably related to mixing within a re-oxygenated water column (Rosales et al., 2006; Korte and Hesselbo, 2011; Silva and Duarte, 2015; Mercuzot et al., 2020).

The T-OAE has been pinpointed at the base of the Nieniexiongla Formation based on multiple lines of evidence: the disappearance of the *Lithiotis Fauna*, changes in sedimentary facies, and carbon- and sulphur-isotope excursions staring at the Pupuga–Nieniexiongla Formation boundary (Fig. 7; ~218 m) (Newton et al., 2011; Han et al., 2016, 2018). Therefore, following the MSBE, the Pliensbachian–Toarcian boundary negative CIE, which has been widely reported in northern Europe, northern Africa and even the palaeo-Pacific Ocean, if everywhere correctly identified (Hesselbo et al., 2007; Suan et al., 2008; Littler et al., 2010; Ait-Itto et al., 2017; Ikeda et al., 2018) would be expected in the interval of ~200 m to ~218 m. However, no carbon-isotope features that could be linked to this event are found at the Wölong and Yunjia sections, probably due to an incomplete stratigraphic record (Figs. 5 and 7). A gap is likely, because a sea-level fall associated with cooling and coincident with the Pliensbachian–Toarcian boundary event is widely reported in west Tethyan and Arctic shelf-sea areas (e.g. Suan et al., 2010; Ruebsam et al., 2019), and also observed in Tibet (Fig. 9; cf. Han et al., 2016).

Another explanation is that this CIE is not a genuine event or at least is a very minor one in terms of carbon-cycle dynamics. Several studies from hemipelagic sections with stratigraphically relatively expanded Pliensbachian successions have failed to observe the peculiar negative CIE at the Pliensbachian-Toarcian boundary or found it much reduced (Hermoso et al., 2009; 2012; Storm et al., 2020). A similar lack of clear signal in coeval $\delta^{13}C$ values from organic matter strongly dominated by terrestrial plant debris is characteristic of three Moroccan sections (Bodin et al. 2016). Nannofossil-rich carbonate in the Peniche section, Portugal (the Global Boundary Stratotype Section and Point for the base of the Toarcian Stage: da Rocha et al., 2016) shows a clear negative carbonate carbon-isotope excursion at the stage boundary, although it is more poorly expressed in associated wood (Hesselbo et al., 2007). Bodin et al. (2016) proposed that the negative CIE primarily expressed in carbonates during the Pliensbachian–Toarcian boundary interval might be related to Tethys-wide collapse of neritic carbonate systems, which would have reduced the input of relatively ^{13}C-rich neritic lime mud into basinal areas and thereby caused a negative $\delta^{13}C_{carb}$ signal in accumulating hemipelagic carbonates. However, given the innate isotopic variability of organic matter that could confound an atmospheric or marine signal, a locally incomplete stratigraphic record of a global event remains a strong possibility.

5.4 The evolution of the Kioto Carbonate Platform

5.4.1 The evolution of facies and depositional environments

In the Wölong section, facies evolution is characterized by a progressive decrease of terrigenous content paralleled by an increase in carbonate (Figs. 8 and 9). This evolution likely testifies to a marine transgression that established the Kioto Carbonate Platform, a large shallow-water sedimentary system that, during the Sinemurian–Pliensbachian interval, was situated on the northern margin of the Indian continent and extended across western Zanskar (India) and eastern southern Tibet (China) (Gaetani and Garzanti, 1991; Jadoul et al., 1998; Sciunnach and Garzanti, 2012; Han et al., 2016, 2018). In terms of stratigraphy, the dominant quartzose sandstone (Fig. 8A), sandy oolitic grainstone/oolitic sandstone (Fig. 8B) facies of the Zhamure Formation, referred to a barrier-island environment, are replaced by the mainly bioclastic and oolitic grainstone carbonate facies (Fig. 8C and D) of the Pupuga Formation (Han et al., 2016). This evolutionary pattern may simply represent the transition from more proximal to more distal open-marine facies caused by sea-level rise in studied area. A significant transgression, possibly related to global warming, is actually documented beginning shortly after the onset of SPBE and is widely documented in the Boreal and Tethyan regions, as well as in southeastern Panthalassa (Legarreta and Uliana, 1996; Hesselbo and Jenkyns, 1998; Korte and Hesselbo, 2011; Haq, 2018).

5.4.2 The possible influence of Early Jurassic key events

Based on the relationship between facies changes and carbon-isotope events in the Wölong section (Fig. 9), carbonates begin to become more prevalent from the level of the SPBE on upwards and mainly contain bioclasts and coated grains, whereas microbial carbonates are nearly absent (cf. Han et al., 2016). This stratigraphic pattern resembles what has been observed in the Trento Platform (northern Italy) in western Tethys where a change in the type of precipitated or secreted carbonate from microbial (prior to the SPBE) to skeletal (after the SPBE) is observed (Franceschi et al., 2019). This change may be seen as possible evidence of a crisis in microbial carbonate production, triggered by the phenomena possibly associated with the SPBE (e.g. ocean acidification, enhanced freshwater input; Franceschi et al., 2019; Jenkyns, 2020) that may have had Tethys wide scale.

Another notable feature observed in the Wölong section is the appearance of large thick-shelled bivalves in the Pupuga Formation of the late Pliensbachian (Figs. 2, 8E, F and 9), which are mainly represented by the lithiotid *Cochlearites* and lesser numbers of *Lithiotis* (cf. Wignall et al., 2006), together named '*Lithiotis* Fauna' in this study by reference to Franceschi et al. (2014) and Posenato et al. (2018). They are important constructors of bioherms and biostromes, and their spread represents a global-scale biocalcification event that is peculiar to the Early Jurassic (e.g. Fraser et al., 2004; Brame et al., 2019). Franceschi et al. (2014) pointed out that the spread of the *Lithiotis* Fauna on the Trento Platform occurred after the SPBE and was synchronous at regional scale. They therefore hypothesized that the amelioration of environmental conditions following a phase of dysoxia, coincident with the SPBE carbon-isotope perturbation, created the meso–oligotrophic conditions suitable for the diffusion of the bivalves. In apparent contrast to this hypothesis, the occurrence of forms referred to the *Lithiotis* Fauna has been reported in the uppermost Sinemurian from Morocco (Danisch et al., 2019). Nevertheless, this age attribution appears debatable because it is based on the presence of the larger benthic foraminifera *Pseudopfenderina butterlini* and *Lituosepta recoarensis*. These two Jurassic species, however, are long-ranging and can be found from the Sinemurian to the Bathonian and the upper Sinemurian to the lower Aalenian, respectively (see BouDagher-Fadel, 2018).

Matching of the stratigraphic distribution of the *Lithiotis* Fauna against the carbon-isotope curve from Wölong, if correlated to the western Tethyan sections of Rocchetta and Viote (Trento Platform, northern Italy: Franceschi et al., 2019), suggests that also on the Kioto Platform the spread of the large bivalves post-dated the rebound of the isotopic values following the SPBE (Fig. 9). In Wölong, the appearance of the *Lithiotis* Fauna roughly corresponds to the onset of the ME that followed shortly after the SPBE. In western Tethyan sections of Italy, the appearance of the *Lithiotis* Fauna also broadly corresponds to a positive shift in $\delta^{13}C_{carb}$ values (Viote around 45 m; Rocchetta around 13 m) that we refer to the ME (Fig. 9). This line of evidence seems to corroborate the hypothesis that the global diffusion of the *Lithiotis* Fauna followed the SPBE and was effectively synchronous at the scale of the entire Tethys, thus strengthening the hypothesis of a connection between the termination of the isotope perturbation and the creation of conditions suitable for the spread of these bivalves. In any event, a possible local appearance of the bivalves of the *Lithiotis* Fauna in the Sinemurian, if confirmed, is not necessarily incompatible with a synchronous large-scale spread. These organisms may have appeared prior to the SPBE, but then may have proliferated only after environmental conditions became more suitable after the isotopic perturbation. More accurate bio-chronostratigraphic constraints on the first occurrence of these bivalves globally are needed to shed further light on this matter.

It is fair to say that massive CO_2 injection into the ocean–atmosphere during the SPBE could have triggered global warming and enhanced nutrient input to the oceans with the development of oxygen-depleted environments, just like the T-OAE (cf. Jenkyns, 2010). The most stressed marine conditions could have exceeded the tolerance levels of *Lithiotis* communities. Such conditions are typically favorable for elevated primary productivity and organic-matter burial. Organic-rich sediments have been reported from the hemipelagic facies of Lusitanian Basin, Portugal (Duarte et al., 2010, 2012), carbonate-ramp facies of Basque–Cantabrian basin, northern Spain (Quesada et al., 1997, 2005; Rosales et al., 2006), and from shallow-water settings of the Trento Platform, Italy (Bassi et al., 1999; Franceschi et al., 2014) during the SPBE, and widely from global sites during the ME, as discussed in section 5.3. Combining the observations from both the eastern and western Tethys, this study leads to the suggestion that the persistent burial of organic matter during the SPBE and ME could have gradually drawn down atmospheric pCO_2 and thus reversed the syn- and post-SPBE greenhouse effect, progressively facilitating the formation of more stable ecosystems. The resultant better oxygenated meso-oligotrophic conditions could have proved favorable for the development and diffusion of the *Lithiotis* Fauna in the entire Tethyan tropics/subtropics immediately following the SPBE and during and after the ME. A further element at play might have been global sea-level rise that is documented shortly after the time of onset of the SPBE (Legarreta and Uliana, 1996; Hesselbo and Jenkyns, 1998; Haq, 2018) and that led to the expansion of carbonate-rich shelf environments, the ecosystem where the *Lithiotis* Fauna thrived.

Foraminiferal data from Wölong highlight an extinction of index taxa, such as *Palaeomayncina termieri, Planisepta compressa,* and *Lituosepta recoarensis*, at the onset level of the MSBE (~177–185 m; Figs. 2 and 8). The skeletal grain content overall shows a decreasing trend through the upper Pliensbachian and reaches a minimum generally consistent with the extinction level (Fig. 9). This event broadly corresponds in timing with the *gibbosus* ammonite subzone biotic crisis in the latest *margaritatus* ammonite zone known from the western Tethys and northeastern Panthalassa (Dera et al., 2010; Caruthers et al., 2014). This association likely suggests a global biotic crisis at the time of the MSBE, although the possible links with the phenomena responsible for the carbon-isotope perturbation are yet to be explored. Subsequently, although a global biotic crisis occurred again at the Pliensbachian–Toarcian boundary (Dera et al., 2010; Caruthers et al., 2014), the variation in LBF and *Lithiotis* Fauna is not clear because of the lack of appropriate records of this event, likely biased by stratigraphic incompleteness due to sea-level fall at this time, as mentioned above. However, *Lithiotis* communities thrived on Pliensbachian shallow-water carbonate platforms in western (Italy and Morocco) and eastern (Tibet) Tethyan regions, suggesting that the environmental and climatic changes associated with the carbon-cycle perturbations did not completely destroy the conditions for skeletal production of carbonates until the early Toarcian (Brame et al., 2019).

6. **Conclusions**

This study presents foraminiferal biostratigraphic, sedimentological and $\delta^{13}C_{carb}$ data from the Lower Jurassic (Sinemurian–lowermost Toarcian) shallow-water carbonates of the Kioto Platform (Tethys Himalaya, Tibet). A total of six foraminiferal zones have been recognized: late Sinemurian *Textulariopsis sinemuriensis,* Pliensbachian *Planisepta compressa, Bosniella oenensis, Cyclorbitopsella tibetica* and *Streptocyclammina liasica,* and earliest Toarcian *Siphovalvulina* sp. A. The foraminiferal biostratigraphic framework and isotope data make it possible to propose a correlation of the $\delta^{13}C$ records of the western Tethyan region and northern Europe. Three carbon-isotope perturbations are identified: the negative $\delta^{13}C$ excursions of the Sinemurian–Pliensbachian boundary event (SPBE) and *margaritatus–spinatum* boundary event (MSBE) and the positive excursion of the margaritatus zone event (ME), mainly in the *margaritatus* zone. The identification of these carbon-isotope perturbations in a section deposited in the austral portion of the Tethys strengthens the global significance of these events.

Facies investigation shows that sedimentary environments in the Tethys Himalaya underwent a transgressive evolution from terrigenous-dominated to mainly carbonate-rich. The carbonate facies that developed at the time of the widespread establishment of the shallow-water carbonate environment of the Kioto Platform, which occurred after the SPBE, are characterized mainly by skeletal grains: a similar pattern to that observed in coeval platform carbonates in the western Tethys. The sediments of the Kioto Platform document the spread of the large bivalves of the *Lithiotis* Fauna. This spread occurred closely following the SPBE, in an analogous way to what has been observed in the western Tethys, suggesting that, following the carbon-isotope perturbation, these organisms could flourish across the whole of the Tethyan region.

There was a global biotic crisis around the onset level of the MSBE, as expressed in this study by extinctions of certain index larger benthic foraminifera. However, *Lithiotis* communities thrived in Tibet (eastern Tethys: southern hemisphere) and in

Morocco and Italy (western Tethys: northern hemisphere) until the early Toarcian, likely recording a general response on the entire shallow-water platform belt.

Acknowledgements

We thank Wei An, Juan Li and Shiyi Li for their assistance in the field, and Yiwei Xu, and Jingxing Jiang for their help in preparing the samples. This study was financially supported by the National Natural Science Foundation of China (nos 41888101, 41525007, 42002121, 41802126), scholarship grant from China Scholarship Council (201706190163), and the program B (201802B079) for Outstanding PhD candidate of Nanjing University. We thank the reviewers, including Mariano Parente (University of Naples), for their constructive comments on the manuscript.

References

Ait-Itto, F.-Z., Price, G.D., Addi, A.A., Chafiki, D., Mannani, I., 2017. Bulk-carbonate and belemnite carbon-isotope records across the Pliensbachian-Toarcian boundary on the northern margin of Gondwana (Issouka, Middle Atlas, Morocco). Palaeogeography, Palaeoclimatology, Palaeoecology 466, 128–136.

Baghli, H., Mattioli, E., Spangenberg, J., Bensalah, M., Arnaud-Godet, F., Pittet, B., Suan, G., 2020. Early Jurassic climatic trends in the south-Tethyan margin. Gondwana Research 77, 67–81.

Barattolo, F., Romano, R., 2005. Shallow carbonate platform bioevents during the Upper Triassic-Lower Jurassic: an evolutive interpretation. Bollettino Della Societa Geologica Italiana 124, 123–142.

Bassi, D., Boomer, I., Fugagnoli, A., Loriga, C., Posenato, R., Whatley, R., 1999. Faunal assemblages and palaeoenvironment of shallow water black shales in the

Tonezza area (Calcari Grigi, Early Jurassic, Southern Alps). Annali dell'Università degli Studi di Ferrara, Sezione di Scienze della Terra 8, 1–16.

Blackburn, T.J., Olsen, P.E., Bowring, S.A., McLean, N.M., Kent, D.V., Puffer, J., McHone, G., Rasbury, E.T., Et-Touhami, M., 2013. Zircon U-Pb Geochronology Links the End-Triassic Extinction with the Central Atlantic Magmatic Province. Science 340, 941–945.

Bodin, S., Krencker, F.N., Kothe, T., Hoffmann, R., Mattioli, E., Heimhofer, U., Kabiri, L., 2016. Perturbation of the carbon cycle during the late Pliensbachian - early Toarcian: New insight from high-resolution carbon isotope records in Morocco. Journal of African Earth Sciences 116, 89–104.

Bond, D.P., Wignall, P.B., 2014. Large igneous provinces and mass extinctions: an update. In: Keller, G., and Kerr, A.C. (eds.). Volcanism, Impacts and Mass Extinctions: Causes and Effects. Geological Society of America Special Papers 505, 29–55.

BouDagher-Fadel, M.K., 2018. Evolution and geological significance of larger benthic foraminifera, second edition. UCL Press, London, 693pp.

BouDagher-Fadel, M.K., Bosence, D.W., 2007. Early Jurassic benthic foraminiferal diversification and biozones in shallow-marine carbonates of western Tethys. Senckenbergiana lethaea 87, 1–39.

Boudagher-Fadel, M.K., Rose, E.P.F., Bosence, D.W.J., Lord, A.R., 2001. Lower Jurassic Foraminifera and Calcified Microflora from Gibraltar, Western Mediterranean. Palaeontology 44, 601–621.

Brame, H.M.R., Martindale, R.C., Ettinger, N.P., Debeljak, I., Vasseur, R., Lathuiliere, B., Kabiri, L., Bodin, S., 2019. Stratigraphic distribution and paleoecological significance of Early Jurassic (Pliensbachian-Toarcian) lithiotid-coral reefal deposits from the Central High Atlas of Morocco. Palaeogeography Palaeoclimatology Palaeoecology 514, 813–837.

Caruthers, A.H., Smith, P.L., Gröcke, D.R., 2014. The Pliensbachian–Toarcian (Early Jurassic) extinction: A North American perspective. In: Keller, G. and Kerr, A.C., Eds, Volcanism, Impacts, and Mass Extinctions: Causes and Effects, Geological Society of America Special Papers 505, 225–243.

Clark, G.N., Boudagher-Fadel, M., 2004. Larger benthic foraminifera and Calcareous algae of the Upper Kesrouane Limestone Formation (Middle/Upper Jurassic) in Central Lebanon; stratigraphy, sedimentology and regional synopsis. Revue De Paleobiologie 23, 477-504.

da Rocha, R., B., Mattioli, E., Duarte, L., Vítor, Pittet, B., Elmi, S., Mouterde, R., Cabral, M.-C., Comas-Rengifo, M., C, Gómez, J., C, Goy, A., C, Hesselbo, S., C, Jenkyns, H., C, Littler, K., C, Mailliot, S., C, Veiga de Oliveira, L.C., Osete, M., Luisa, Perilli, N., P, Pinto, S., C, Ruget, C., C, Suan, G., C, 2016. Base of the Toarcian Stage of the Lower Jurassic defined by the Global Boundary Stratotype Section and Point (GSSP) at the Peniche section (Portugal). Episodes 39, 460–481.

Danisch, J., Kabiri, L., Nutz, A., Bodin, S., 2019. Chemostratigraphy of Late Sinemurian – Early Pliensbachian shallow-to deep-water deposits of the Central High Atlas Basin: Paleoenvironmental implications. Journal of African Earth Sciences 153, 239–249.

De Lena, L.F., Taylor, D., Guex, J., Bartolini, A., Adatte, T., van Acken, D., Spangenberg, J.E., Samankassou, E., Vennemann, T., Schaltegger, U., 2019. The driving mechanisms of the carbon cycle perturbations in the late Pliensbachian (Early Jurassic). Scientific Reports 9, 18430.

Dera, G., Brigaud, B., Monna, F., Laffont, R., Puceat, E., Deconinck, J.F., Pellenard, P., Joachimski, M.M., Durlet, C., 2011. Climatic ups and downs in a disturbed Jurassic world. Geology 39, 215–218.

Dera, G., Neige, P., Dommergues, J.-L., Fara, E., Laffont, R., Pellenard, P., 2010. High-resolution dynamics of Early Jurassic marine extinctions: the case of Pliensbachian–Toarcian ammonites (Cephalopoda). Journal of the Geological Society 167, 21–33.

Duarte, L.V., Comas-Rengifo, M.J., Silva, R.L., Paredes, R., Goy, A., 2014. Carbon isotope stratigraphy and ammonite biochronostratigraphy across the Sinemurian-Pliensbachian boundary in the western Iberian margin. Bulletin of Geosciences 89, 719–736.

Duarte, L.V., Oliveira, L., Comas-Rengifo, M.J., Silva, F., Silva, R.L., 2010. Organic-Rich facies in the Sinemurian and Pliensbachian of the Lusitanian Basin, Portugal: total organic carbon distribution and relation to transgressive-regressive facies cycles. Geologica Acta 8, 325–340.

Duarte, L.V., Silva, R.L., Filho, J.G.M., Ribeiro, N.P., Chagas, R., 2012. High-resolution stratigraphy, palynofacies and source rock potential of the Água de Madeiros Formation (Lower Jurassic), Lusitanian Basin, Portugal. Journal of Petroleum Geology 35, 105–126.

Flügel, E., 2010. Microfacies of carbonate rocks: analysis, interpretation and application, 2nd edn. Springer-Verlag, Berlin Heidelberg New York. pp. 1–984.

Franceschi, M., Dal Corso, J., Posenato, R., Roghi, G., Masetti, D., Jenkyns, H.C., 2014. Early Pliensbachian (Early Jurassic) C-isotope perturbation and the diffusion of the Lithiotis Fauna: insights from the western Tethys. Palaeogeography, Palaeoclimatology, Palaeoecology 410, 255–263.

Franceschi, M., Dal Corso, J., Cobianchi, M., Roghi, G., Penasa, L., Picotti, V., Preto, N., 2019. Tethyan carbonate platform transformations during the Early Jurassic (Sinemurian− Pliensbachian, Southern Alps): Comparison with the Late Triassic Carnian Pluvial Episode. Geological Society of America Bulletin 131, 1255–1275.

Fraser, N.M., Bottjer, D.J., Fischer, A.G., 2004. Dissecting "*Lithiotis*" bivalves: implications for the Early Jurassic reef eclipse. Palaios 19, 51–67.

Gaetani, M., Garzanti, E., 1991. Multicyclic history of the Northern India continental margin (Northwestern Himalaya). American Association of Petroleum Geologists Bulletin 75, 1427–1446.

Gale, L., Barattolo, F., Rettori, R., 2018. Morphometric approach to determination of lower Jurassic siphovalvulinid foraminifera. Rivista Italiana di Paleontologia e Stratigrafia 124, 265–282.

Golonka, J., 2007. Phanerozoic Paleoenvironment and Paleolithofacies Maps. Mesozoic. Geologia 35, 589–654.

Han, Z., Hu, X., Kemp, D.B., Li, J., 2018. Carbonate-platform response to the Toarcian Oceanic Anoxic Event in the southern hemisphere: Implications for climatic change and biotic platform demise. Earth and Planetary Science Letters 489, 59–71.

Han, Z., Hu, X.M., Li, J., Garzanti, E., 2016. Jurassic carbonate microfacies and relative sea-level changes in the Tethys Himalaya (southern Tibet). Palaeogeography Palaeoclimatology Palaeoecology 456, 1–20.

Haq, B.U., 2018. Jurassic Sea-Level Variations: A Reappraisal. GSA Today 28, https://doi.org/10.1130/GSATG1359A.1131.

Harazim, D., van de Schootbrugge, B., Sorichter, K., Fiebig, J., Weug, A., Suan, G., Oschmann, W., 2013. Spatial variability of watermass conditions within the European Epicontinental Seaway during the Early Jurassic (Pliensbachian–

Toarcian). Sedimentology 60, 359–390.

Hermoso, M., Le Callonnec, L., Minoletti, F., Renard, M., Hesselbo, S.P., 2009. Expression of the Early Toarcian negative carbon-isotope excursion in separated carbonate microfractions (Jurassic, Paris Basin). Earth and Planetary Science Letters 277, 194–203.

Hermoso, M., Minoletti, F., Rickaby, R.E.M., Hesselbo, S.P., Baudin, F., Jenkyns, H.C., 2012. Dynamics of a stepped carbon-isotope excursion: Ultra high-resolution study of Early Toarcian environmental change. Earth and Planetary Science Letters 319, 45–54.

Hesselbo, S.P., Jenkyns, H.C., 1998. British lower Jurassic sequence stratigraphy. In: de Graciansky, P.-C., Hardenbol, J., Jacquin, T., Vail, P.R. (Eds), Mesozoic and Cenozoic Sequence Stratigraphy of European Basins, Special Publication Society for Sedimentary Geology (SEPM) 60, 561–581.

Hesselbo, S.P., Jenkyns, H.C., Duarte, L.V., Oliveira, L.C.V., 2007. Carbon-isotope record of the Early Jurassic (Toarcian) Oceanic Anoxic Event from fossil wood and marine carbonate (Lusitanian Basin, Portugal). Earth and Planetary Science Letters 253, 455–470.

Huang, W.T., van Hinsbergen, D.J., Dekkers, M.J., Garzanti, E., Dupont-Nivet, G., Lippert, P.C., Li, X.C., Maffione, M., Langereis, C.G., Hu, X.M., 2015. Paleolatitudes of the Tibetan Himalaya from primary and secondary magnetizations of Jurassic to Lower Cretaceous sedimentary rocks. Geochemistry, Geophysics, Geosystems 16, 77–100.

Ikeda, M., Hori, R.S., Ikehara, M., Miyashita, R., Chino, M., Yamada, K., 2018. Carbon cycle dynamics linked with Karoo-Ferrar volcanism and astronomical cycles during Pliensbachian-Toarcian (Early Jurassic). Global and Planetary Change 170, 163–171.

Jadoul, F., Berra, F., Garzanti, E., 1998. The Tethys Himalayan passive margin from Late Triassic to Early Cretaceous (South Tibet). Journal of Asian Earth Sciences 16, 173–194.

Jenkyns, H.C., 2010. Geochemistry of oceanic anoxic events. Geochemistry Geophysics Geosystems 11, Q03004, doi: 10.1029/2009GC002788.

Jenkyns, H.C., 2020. The demise and drowning of Early Jurassic (Sinemurian) carbonate platforms: stratigraphic evidence from the Italian peninsula, Sicily and Spain. In: l' Eredità scientifica di Paolo Scandone, Geologo, Atti del Convegni Lincei, 335, 55–82.

Jenkyns, H.C., Clayton, C.J., 1986. Black shales and carbon isotopes in pelagic sediments from the Tethyan Lower Jurassic. Sedimentology 33, 87–106.

Jenkyns, H.C., Clayton, C.J., 1997. Lower Jurassic epicontinental carbonates and mudstones from England and Wales: chemostratigraphic signals and the early Toarcian anoxic event. Sedimentology 44, 687–706.

Jenkyns, H.C., Jones, C.E., Grocke, D.R., Hesselbo, S.P., Parkinson, D.N., 2002. Chemostratigraphy of the Jurassic System: applications, limitations and implications for palaeoceanography. Journal of the Geological Society 159, 351–378.

Kaufman, A.J., Knoll, A.H., 1995. Neoproterozoic variations in the C-isotopic composition of seawater: stratigraphic and biogeochemical implications. Precambrian Research 73, 27–49.

Korte, C., Hesselbo, S.P., 2011. Shallow marine carbon and oxygen isotope and elemental records indicate icehouse-greenhouse cycles during the Early Jurassic. Paleoceanography 26, PA4219, doi: 10.1029/2011PA002160.

Korte, C., Hesselbo, S.P., Ullmann, C.V., Dietl, G., Ruhl, M., Schweigert, G., Thibault, N., 2015. Jurassic climate mode governed by ocean gateway. Nature Communications 6, 10015.

Legarreta, L., Uliana, M.A., 1996. The Jurassic succession in west-central Argentina: stratal patterns, sequences and paleogeographic evolution. Palaeogeography, Palaeoclimatology, Palaeoecology 120, 303–330.

Leinfelder, R.R., Schmid, D.U., Nose, M., Werner, W., 2002. Jurassic reef patterns-the expression of a changing globe. In: Kiessling, W., Flügel, E. and Golonka, J, Eds, Phanerozoic Reef Patterns, Society for Sedimentary Geology (SEPM). Special Publication 72, 465–520.

Littler, K., Hesselbo, S.P., Jenkyns, H.C., 2010. A carbon-isotope perturbation at the Pliensbachian-Toarcian boundary: evidence from the Lias Group, NE England. Geological Magazine 147, 181–192.

Liu, G.H., Einsele, G., 1994. Sedimentary history of the Tethyan basin in the Tibetan Himalayas. Geologische Rundschau 83, 32–61.

Marshall, J.D., 1992. Climatic and oceanographic isotopic signals from the carbonate rock record and their preservation. Geological Magazine 129, 143–160.

Mercuzot, M., Pellenard, P., Christophe, D., Bougeault, C., Meister, C., Dommergues, J.-L., Thibault, N., Baudin, F., Mathieu, O., Bruneau, L., Huret, E., Hmidi, K., 2019. Carbon-isotope events during the Pliensbachian (Lower Jurassic) on the African and European margins of the NW Tethyan Realm. Newsletters on Stratigraphy 53, 41–69.

Newton, R.J., Reeves, E.P., Kafousia, N., Wignall, P.B., Bottrell, S.H., Sha, J.-G., 2011. Low marine sulfate concentrations and the isolation of the European epicontinental sea during the Early Jurassic. Geology 39, 7–10.

Page, K.N., 2003. The Lower Jurassic of Europe: its subdivision and correlation. Geological Survey of Denmark and Greenland Bulletin 1, 21–59.

Pálfy, J., Smith, P.L., 2000. Synchrony between Early Jurassic extinction, oceanic anoxic event, and the Karoo-Ferrar flood basalt volcanism. Geology 28, 747–750.

Percival, L.M.E., Witt, M.L.I., Mather, T.A., Hermoso, M., Jenkyns, H.C., Hesselbo, S.P., Al-Suwaidi, A.H., Storm, M.S., Xu, W., Ruhl, M., 2015. Globally enhanced mercury deposition during the end-Pliensbachian extinction and Toarcian OAE: A link to the Karoo-Ferrar Large Igneous Province. Earth and Planetary Science Letters 428, 267–280.

Percival, L.M., Ruhl, M., Hesselbo, S.P., Jenkyns, H.C., Mather, T.A., Whiteside, J.H., 2017. Mercury evidence for pulsed volcanism during the end-Triassic mass extinction. Proceedings of the National Academy of Sciences 114, 7929–7934.

Peti, L., Thibault, N., Clémence, M.-E., Korte, C., Dommergues, J.-L., Bougeault, C., Pellenard, P., Jelby, M.E., Ullmann, C.V., 2017. Sinemurian–Pliensbachian calcareous nannofossil biostratigraphy and organic carbon isotope stratigraphy in the Paris Basin: Calibration to the ammonite biozonation of NW Europe. Palaeogeography, Palaeoclimatology, Palaeoecology 468, 142–161.

Posenato, R., Bassi, D., Trecalli, A., Parente, M., 2018. Taphonomy and evolution of Lower Jurassic lithiotid bivalve accumulations in the Apennine Carbonate Platform (southern Italy). Palaeogeography Palaeoclimatology Palaeoecology 489, 261–271.

Posenato, R., Masetti, D., 2012. Environmental control and dynamics of Lower Jurassic bivalve build-ups in the Trento Platform (Southern Alps, Italy). Palaeogeography Palaeoclimatology Palaeoecology 361, 1–13.

Price, G.D., Baker, S.J., VanDeVelde, J., Clemence, M.E., 2016. High-resolution carbon cycle and seawater temperature evolution during the Early Jurassic (Sinemurian-Early Pliensbachian). Geochemistry Geophysics Geosystems 17, 3917–3928.

Quesada, S., Dorronsoro, C., Robles, S., Chaler, R., Grimalt, J.O., 1997. Geochemical correlation of oil from the Ayoluengo field to Liassic black shale units in the southwestern Basque-Cantabrian Basin (northern Spain). Organic Geochemistry 27, 25–40.

Quesada, S., Robles, S., Rosales, I., 2005. Depositional architecture and transgressive–regressive cycles within Liassic backstepping carbonate ramps in the Basque–Cantabrian basin, northern Spain. Journal of the Geological Society 162, 531–548.

Rosales, I., Quesada, S., Robles, S., 2004. Paleotemperature variations of Early Jurassic seawater recorded in geochemical trends of belemnites from the Basque–Cantabrian basin, northern Spain. Palaeogeography, Palaeoclimatology, Palaeoecology 203, 253–275.

Rosales, I., Quesada, S., Robles, S., 2006. Geochemical arguments for identifying second-order sea-level changes in hemipelagic carbonate ramp deposits. Terra Nova 18, 233–240.

Ruebsam, W., Mayer, B., Schwark, L., 2019. Cryosphere carbon dynamics control early Toarcian global warming and sea level evolution. Global and Planetary Change 172, 440–453.

Ruhl, M., Hesselbo, S.P., Al-Suwaidi, A., Jenkyns, H.C., Damborenea, S.E., Manceñido, M.O., Storm, M., Mather, T.A., Riccardi, A.C., 2020. On the onset of Central Atlantic Magmatic Province (CAMP) volcanism and environmental and carbon-cycle change at the Triassic–Jurassic transition (Neuquén Basin, Argentina). Earth-Science Reviews 208, 103229.

Ruhl, M., Hesselbo, S.P., Hinnov, L., Jenkyns, H.C., Xu, W., Riding, J.B., Storm, M., Minisini, D., Ullmann, C.V., Leng, M.J., 2016. Astronomical constraints on the duration of the Early Jurassic Pliensbachian Stage and global climatic fluctuations. Earth and Planetary Science Letters 455, 149–165.

Scholle, P.A., Arthur, M.A., 1980. Carbon Isotope Fluctuations in Cretaceous Pelagic Limestones: Potential Stratigraphic and Petroleum Exploration Tool1. American Association of Petroleum Geologists Bulletin 64, 67–87.

Schöllhorn, I., Adatte, T., Van de Schootbrugge, B., Houben, A., Charbonnier, G., Janssen, N., Föllmi, K.B., 2020. Climate and environmental response to the break-up of Pangea during the Early Jurassic (Hettangian-Pliensbachian); the Dorset coast (UK) revisited. Global and Planetary Change 185, 103096.

Sciunnach, D., Garzanti, E., 2012. Subsidence history of the Tethys Himalaya. Earth-Science Reviews 111, 179–198.

Silva, R.L., Duarte, L.V., 2015. Organic matter production and preservation in the Lusitanian Basin (Portugal) and Pliensbachian climatic hot snaps. Global and Planetary Change 131, 24–34.

Silva, R.L., Duarte, L.V., Comas-Rengifo, M.J., Mendonça Filho, J.G., Azerêdo, A.C., 2011. Update of the carbon and oxygen isotopic records of the Early–Late Pliensbachian (Early Jurassic, ~187Ma): Insights from the organic-rich hemipelagic series of the Lusitanian Basin (Portugal). Chemical Geology 283, 177–184.

Storm, M.S., Hesselbo, S.P., Jenkyns, H.C., Ruhl, M., Ullmann, C.V., Xu, W., Leng, M.J., Riding, J.B., Gorbanenko, O., 2020. Orbital pacing and secular evolution of the Early Jurassic carbon cycle. Proceedings of the National Academy of Sciences of the United States of America 117, 3974–3982.

Suan, G., Mattioli, E., Pittet, B., Lecuyer, C., Sucheras-Marx, B., Duarte, L.V., Philippe, M., Reggiani, L., Martineau, F., 2010. Secular environmental precursors to Early Toarcian (Jurassic) extreme climate changes. Earth and Planetary Science Letters 290, 448–458.

Suan, G., Mattioli, E., Pittet, B., Mailliot, S., Lecuyer, C., 2008. Evidence for major environmental perturbation prior to and during the Toarcian (Early Jurassic) oceanic anoxic event from the Lusitanian Basin, Portugal. Paleoceanography 23, PA001459, doi: 10.1029/2007PA001459.

Suan, G., Nikitenko, B.L., Rogov, M.A., Baudin, F., Spangenberg, J.E., Knyazev, V.G., Glinskikh, L.A., Goryacheva, A.A., Adatte, T., Riding, J.B., Follmi, K.B., Pittet, B., Mattioli, E., Lecuyer, C., 2011. Polar record of Early Jurassic massive carbon injection. Earth and Planetary Science Letters 312, 102–113.

Swart, P.K., Oehlert, A.M., 2018. Revised interpretations of stable C and O patterns in carbonate rocks resulting from meteoric diagenesis. Sedimentary Geology 364, 14–23.

van de Schootbrugge, B., Bailey, T.R., Rosenthal, Y., Katz, M.E., Wright, J.D., Miller, K.G., Feist-Burkhardt, S., Falkowski, P.G., 2005. Early Jurassic climate change and the radiation of organic-walled phytoplankton in the Tethys Ocean. Paleobiology 31, 73–97.

Wignall, P.B., Hallam, A., Newton, R.J., Sha, J.G., Reeves, E., Mattioli, E., Crowley, S., 2006. An eastern Tethyan (Tibetan) record of the Early Jurassic (Toarcian) mass extinction event. Geobiology 4, 179–190.

Woodfine, R.G., Jenkyns, H.C., Sarti, M., Baroncini, F., Violante, C., 2008. The response of two Tethyan carbonate platforms to the early Toarcian (Jurassic) oceanic anoxic event: environmental change and differential subsidence.

Sedimentology 55, 1011–1028.

Figure captions

Fig. 1. (A) Early Jurassic palaeogeographic map of the Tethys Ocean, modified after Golonka (2007) and Han et al. (2018). (B) Detailed road map showing the studied section, modified after Han et al. (2016), and also the location of the nearby Yunjia section studied by Wignall et al. (2006) and Newton et al. (2011), ~500 m away from the Wölong section. Y: Yorkshire, Cleveland Basin; M: Mochras Core, Cardigan Bay Basin. S: Sancerre core, Paris Basin, France; P: Peniche, Lusitanian Basin; A: Algeria, T: Trento Carbonate Platform; K: Kioto Carbonate Platform.

Fig. 2. Lithological log, after Han et al. (2016), and biostratigraphic framework and foraminiferal distribution chart of the Wölong section on the Kioto Platform. *Lithiotis* Fauna data are from Jadoul et al. (1998) and Han et al. (2016, 2018) for the Wölong section; larger benthic foraminiferal zones are established based on BouDagher-Fadel (2018). Foraminifera disappearing at 177–185 m, namely at the onset level of the MSBE (see Figs. 5 and 8 for details), are marked in purple rectangles.

Fig. 3. Index foraminiferal species of the Wölong section. A: *Siphovalvulina colomi* BouDagher-Fadel, Rose, Bosence and Lord; B: *Rectocyclammina* sp.; C: *Everticyclammina praevirguliana* Fugagnoli; D: *Lituosepta recoarensis*; E: *Bosniella oenensis* Gušic; F: *Cyclorbitopsella tibetica* Cherchi, Schroeder and Zhang; G: *Orbitopsella prilpeva*; H: *Orbitopsella praecursor* (Gümbel); I: *Planisepta compressa* (Hottinger); J: *Streptocyclammina liasica* Hottinger; K: *Palaeomayncina termieri*; L: *Siphovalvulina* sp. A; M: *Mesoendothyra* cf. *croatica* Gušic. Scale bars: Fig. A =

0.15mm; Figs. B-E, G, K, L = 0.5mm; Figs. F, H-J, M = 1mm.

Fig. 4. Proposed correlation between LBF zones and *Lithiotis* Fauna of the Wölong section, and standard Tethyan and Boreal ammonite zones of the Lower Jurassic. Ammonite zones are after Page (2003) and correlation is according to BouDagher-Fadel (2018). Abbreviations: Sin. = Sinemurian; Toar. = Toarcian; Biv. = Bivalve.

Fig. 5. Carbon-isotope correlation between the Wölong (A, this study) and Yunjia (B, Wignall et al., 2006) sections based on the position of the top *Lithiotis* Fauna horizon and the Pupuga–Nieniexiongla Formations boundary, i.e., the Toarcian maximum flooding surface and abrupt facies change (black dashed line, Han et al., 2016, 2018). $\delta^{13}C_{carb}$ profile of the Wölong section has been illustrated with characteristic microfacies. 1. (black data points): Finely crystalline dolostone; 2 (red data points): Micrite; 3 (blue data points): Wackestone/Packstone; 4 (green data points): Grainstone; 5 (purple data points): Mixed carbonate–siliciclastic deposits. Note that these two outcrops can be combined into one composite section because of their close proximity to one another. B. a. z. equivalent = Boreal ammonite zone equivalent.

Fig. 6. Correlation between $\delta^{13}C_{carb}$ and $\delta^{18}O_{carb}$ (A) and box-plot (B) showing the relationship between isotopic values and facies of the studied samples.

Fig. 7. Carbon-isotope chemostratigraphical correlation between the Wölong (this study) and Yunjia (Wignall et al., 2006) sections in Tibet and characteristic profiles reported from the Mochras core, Cardigan Bay Basin, Wales, UK (Storm et al., 2020), Cleveland Basin, UK (green data points, Ruhl et al., 2016, and black and blue data points, Korte and Hesselbo, 2011), and Trento Platform, northern Italy (Franceschi et

al., 2019). SPBE: Sinemurian–Pliensbachian boundary event; MSBE: *margaritatus*–*spinatum* boundary event; ME: *margaritatus* zone event, mainly in the *margaritatus* zone. Mbs: metres below surface.

Fig. 8. Microfacies and *Lithiotis* Fauna from the Wölong section. **A:** Quartzose sandstone (~2 m); B: Sandy oolitic grainstone/oolitic sandstone (~87 m), with larger foraminiferan *Lituosepta recoarensis*; C: Bioclastic grainstone (~193 m), including diverse fragments of bivalves, foraminifera, brachiopods, echinoderms, etc.; D: Oolitic grainstone (~205 m), displaying strong micritization of ooids and bioclasts; E: *Lithiotis* Fauna in the lower section (~150 m); F: *Lithiotis* Fauna in the upper section (~198 m).

Fig. 9. Quartz and carbonate skeletal grain abundance (this study), relative sea-level (RSL) changes constructed by microfacies analysis (Wölong section, Han et al., 2016), and *Lithiotis*–chemostratigraphic correlation between the Kioto (Wölong section, this study) and Trento (Italy, Franceschi et al., 2014) Platforms during the Sinemurian–Pliensbachian interval. Qg: Quartz grains; Sg: Skeletal grains.

Fig. 1

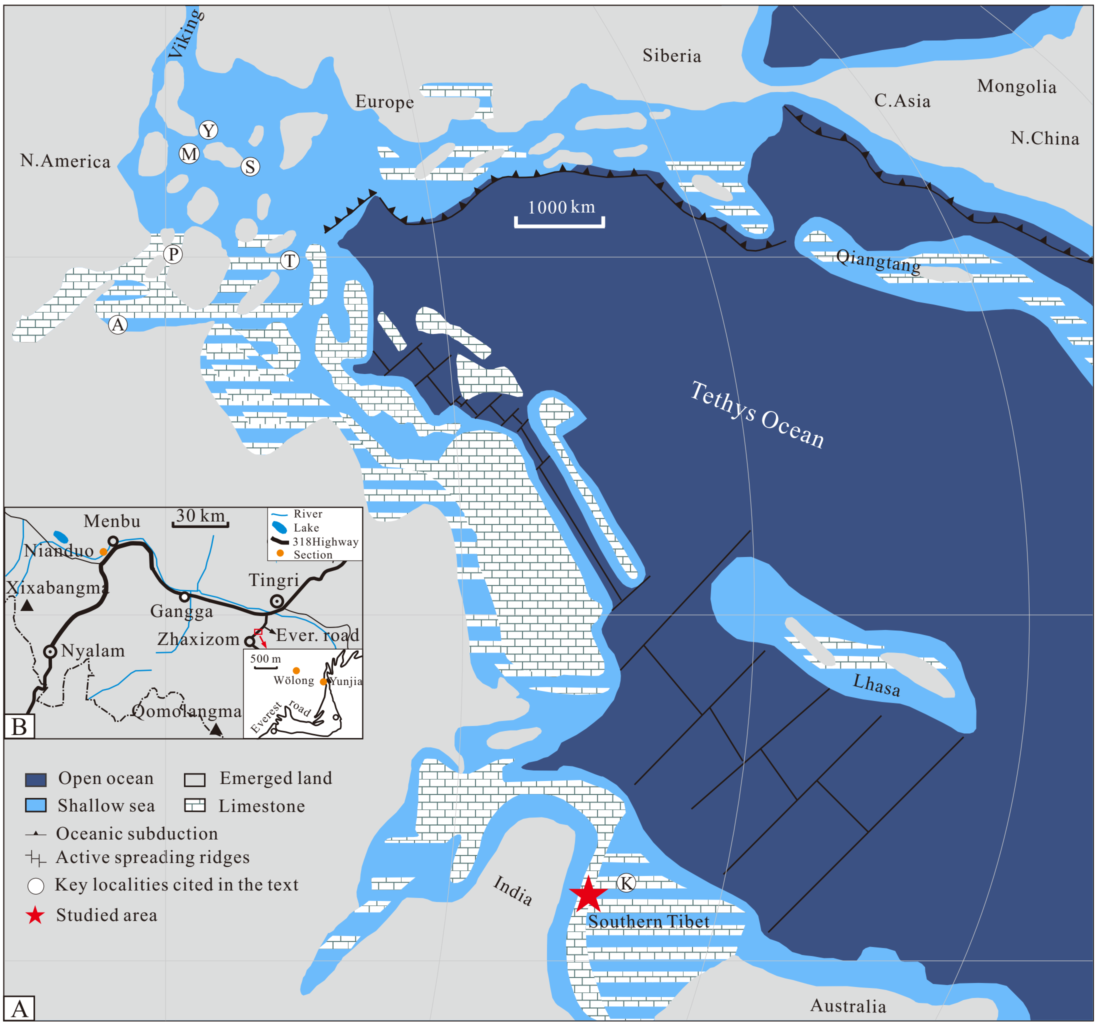

Viking
Europe
Siberia
C.Asia
Mongolia
N.China
N.America
Y
M
S
P
T
A
1000 km
Qiangtang
Tethys Ocean
Lhasa
India
K
Southern Tibet
Australia
30°
0°
30°
Menbu
30 km
River
Lake
318Highway
Section
Nianduo
Xixabangma
Tingri
Gangga
Zhaxizom
Ever. road
Nyalam
500 m
Wölong
Yunjia
Everest road
Qomolangma
B
Open ocean
Shallow sea
Emerged land
Limestone
Oceanic subduction
Active spreading ridges
Key localities cited in the text
Studied area
A

Fig. 2

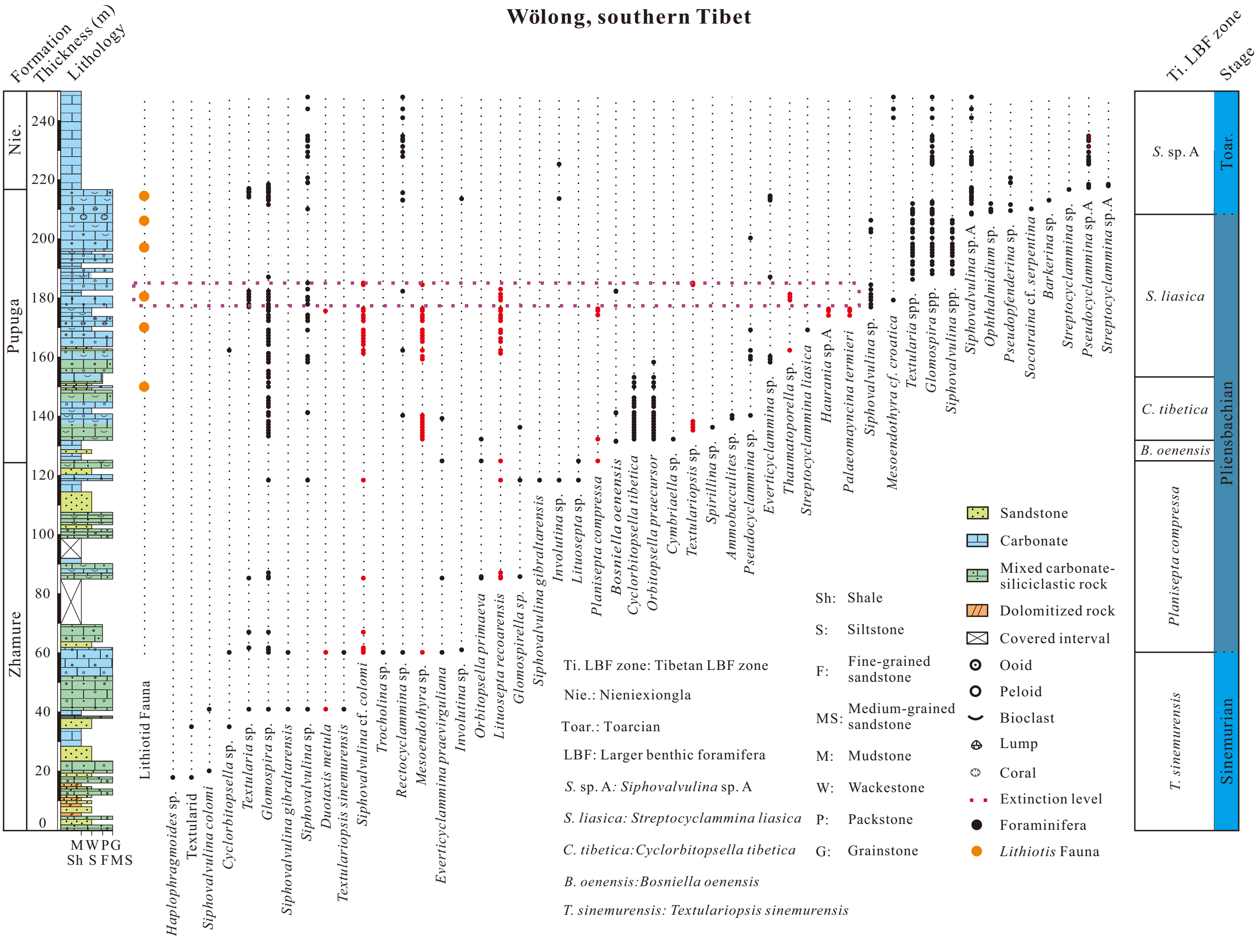

Wölong, southern Tibet
Formation
Thickness (m)
Lithology
Ti. LBF zone
Stage
Nie.
Pupuga
Zhamure
0
20
40
60
80
100
120
140
160
180
200
220
240
M W P G
Sh S F MS
Lithiotid Fauna
Haplophragmoides sp.
Textularid
Siphovalvulina colomi
Cyclorbitopsella sp.
Textularia sp.
Glomospira sp.
Siphovalvulina gibraltarensis
Siphovalvulina sp.
Duotaxis metula
Textulariopsis sinemurensis
Siphovalvulina cf. colomi
Trocholina sp.
Rectocyclammina sp.
Mesoendothyra sp.
Everticyclammina praevirguliana
Involutina sp.
Orbitopsella primaeva
Lituosepta recoarensis
Glomospirella sp.
Siphovalvulina gibraltarensis
Involutina sp.
Lituosepta sp.
Planisepta compressa
Bosniella oenensis
Cyclorbitopsella tibetica
Orbitopsella praecursor
Cymbriaella sp.
Textulariopsis sp.
Spirillina sp.
Ammobaculites sp.
Pseudocyclammina sp.
Everticyclammina sp.
Thaumatoporella sp.
Streptocyclammina liasica
Haurania sp.A
Palaeomayncina termieri
Siphovalvulina sp.
Mesoendothyra cf. croatica
Textularia spp.
Glomospira spp.
Siphovalvulina spp.
Siphovalvulina sp.A
Ophthalmidium sp.
Pseudopfenderina sp.
Socotraina cf. serpentina
Barkerina sp.
Streptocyclammina sp.
Pseudocyclammina sp.A
Streptocyclammina sp.A
S. sp. A
S. liasica
C. tibetica
B. oenensis
Planisepta compressa
T. sinemurensis
Toar.
Pliensbachian
Sinemurian
Ti. LBF zone: Tibetan LBF zone
Nie.: Nieniexiongla
Toar.: Toarcian
LBF: Larger benthic foraminifera
S. sp. A: Siphovalvulina sp. A
S. liasica: Streptocyclammina liasica
C. tibetica: Cyclorbitopsella tibetica
B. oenensis: Bosniella oenensis
T. sinemurensis: Textulariopsis sinemurensis
Sh: Shale
S: Siltstone
F: Fine-grained sandstone
MS: Medium-grained sandstone
M: Mudstone
W: Wackestone
P: Packstone
G: Grainstone
Sandstone
Carbonate
Mixed carbonate-siliciclastic rock
Dolomitized rock
Covered interval
Ooid
Peloid
Bioclast
Lump
Coral
Extinction level
Foraminifera
Lithiotis Fauna

Fig. 3

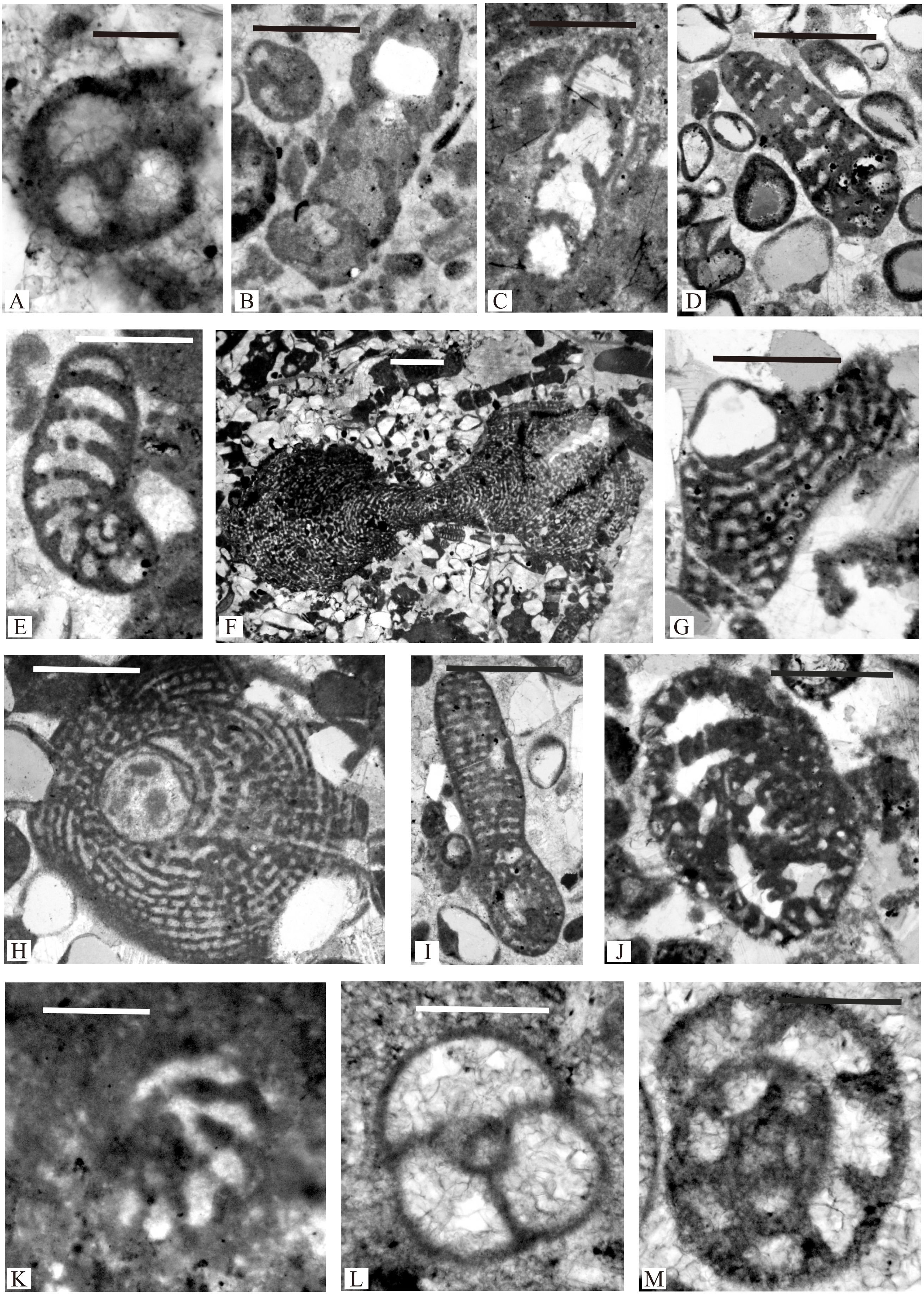

Fig. 4

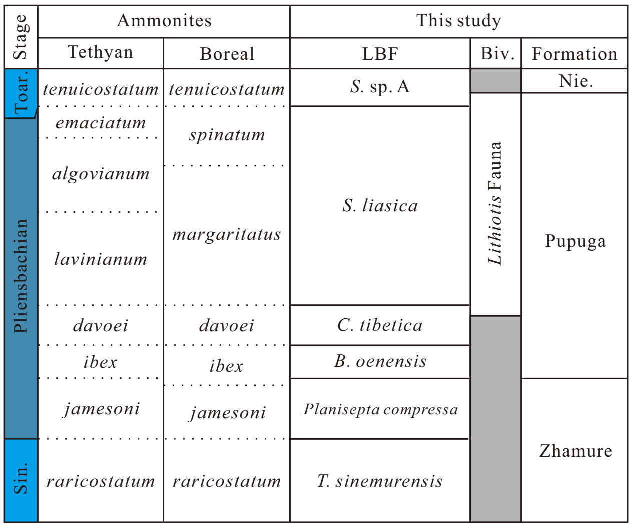

Stage
Ammonites
This study
Tethyan
Boreal
LBF
Biv.
Formation
Toar.
Pliensbachian
Sin.
tenuicostatum
emaciatum
algovianum
lavinianum
davoei
ibex
jamesoni
raricostatum
tenuicostatum
spinatum
margaritatus
davoei
ibex
jamesoni
raricostatum
S. sp. A
S. liasica
C. tibetica
B. oenensis
Planisepta compressa
T. sinemurensis
Lithiotis Fauna
Nie.
Pupuga
Zhamure

Fig. 5

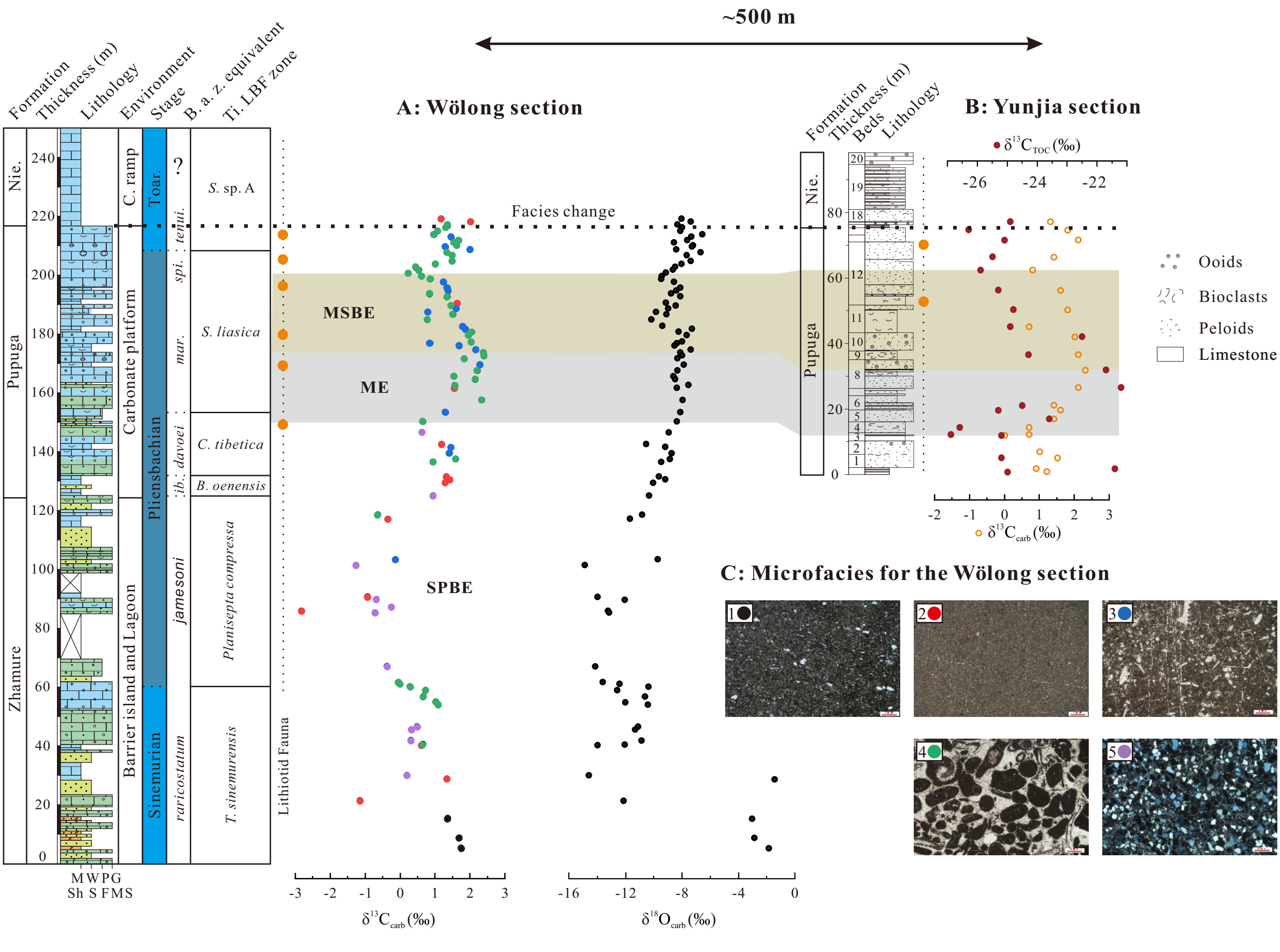
~500 m
A: Wölong section
B: Yunjia section
C: Microfacies for the Wölong section
Formation
Thickness (m)
Lithology
Environment
Stage
B. a. z. equivalent
Ti. LBF zone
Nie.
Pupuga
Zhamure
C. ramp
Carbonate platform
Barrier island and Lagoon
Toar.
Pliensbachian
Sinemurian
tenui.
spi.
mar.
davoei
ib.
jamesoni
raricostatum
S. sp. A
S. liasica
C. tibetica
B. oenensis
Planisepta compressa
T. sinemurensis
Lithiotid Fauna
Facies change
MSBE
ME
SPBE
M W P G
Sh S F M S
δ13Ccarb (‰)
δ18Ocarb (‰)
Beds
δ13CTOC (‰)
Ooids
Bioclasts
Peloids
Limestone

Fig. 6

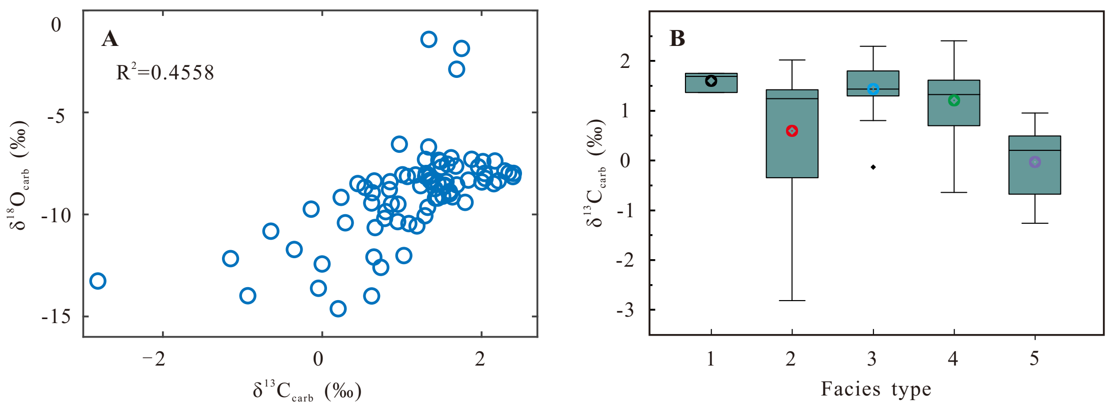

A
R^2=0.4558
0
-5
-10
-15
−2
0
2
$\delta^{18}O_{carb}$ (‰)
$\delta^{13}C_{carb}$ (‰)
B
2
1
0
-1
-2
-3
1
2
3
4
5
$\delta^{13}C_{carb}$ (‰)
Facies type

Fig. 7

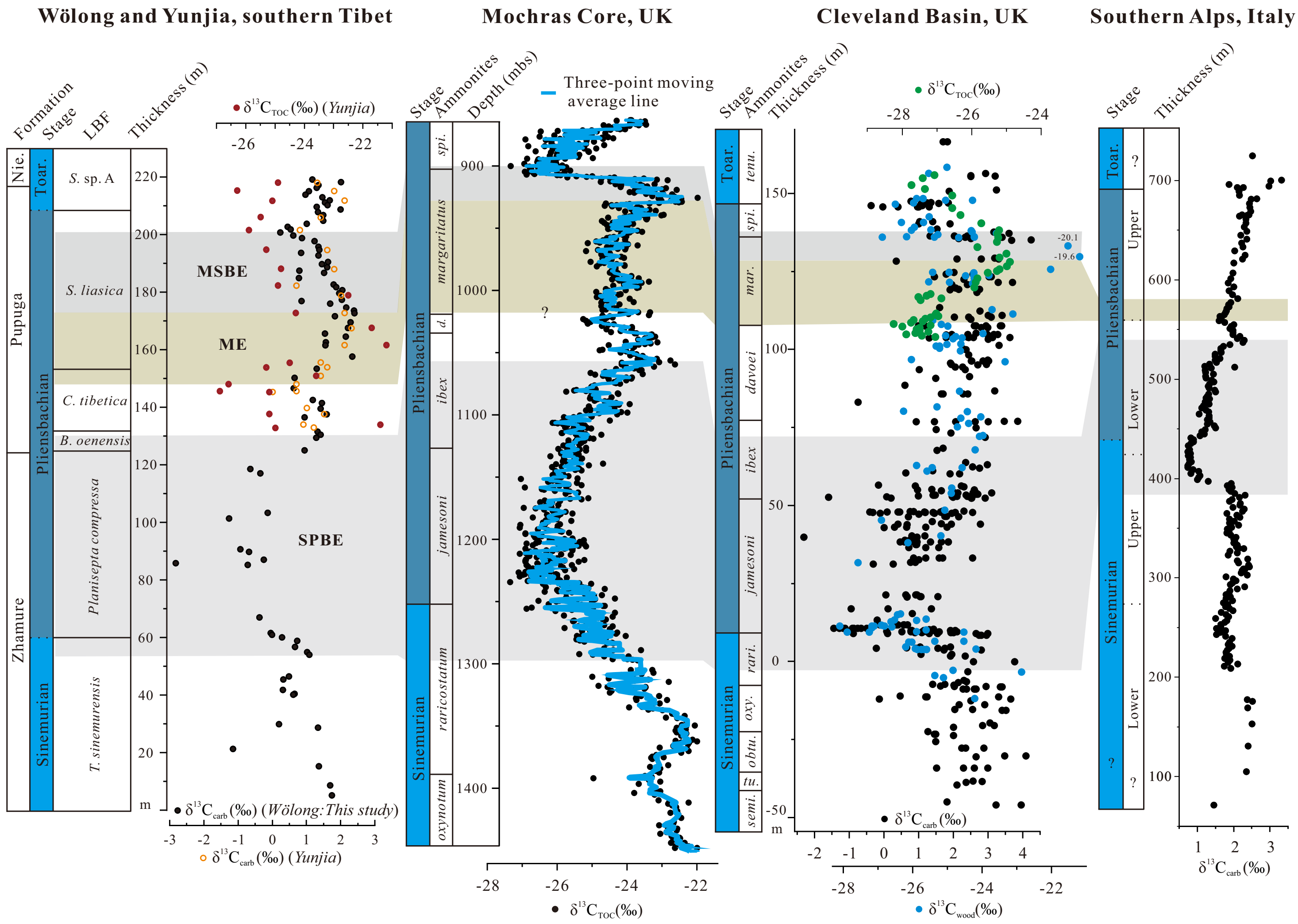

Wölong and Yunjia, southern Tibet
Mochras Core, UK
Cleveland Basin, UK
Southern Alps, Italy
Formation
Stage
LBF
Thickness (m)
δ13C TOC (‰) (Yunjia)
δ13C carb (‰) (Wölong: This study)
δ13C carb (‰) (Yunjia)
Nie.
Toar.
Pupuga
Zhamure
Pliensbachian
Sinemurian
S. sp. A
S. liasica
C. tibetica
B. oenensis
Planisepta compressa
T. sinemurensis
MSBE
ME
SPBE
Ammonites
Depth (mbs)
Three-point moving average line
spi.
margaritatus
d.
ibex
jamesoni
raricostatum
oxynotum
δ13C TOC (‰)
tenu.
mar.
davoei
rari.
oxy.
obtu.
tu.
semi.
δ13C wood (‰)
-20.1
-19.6
Upper
Lower

Fig. 8

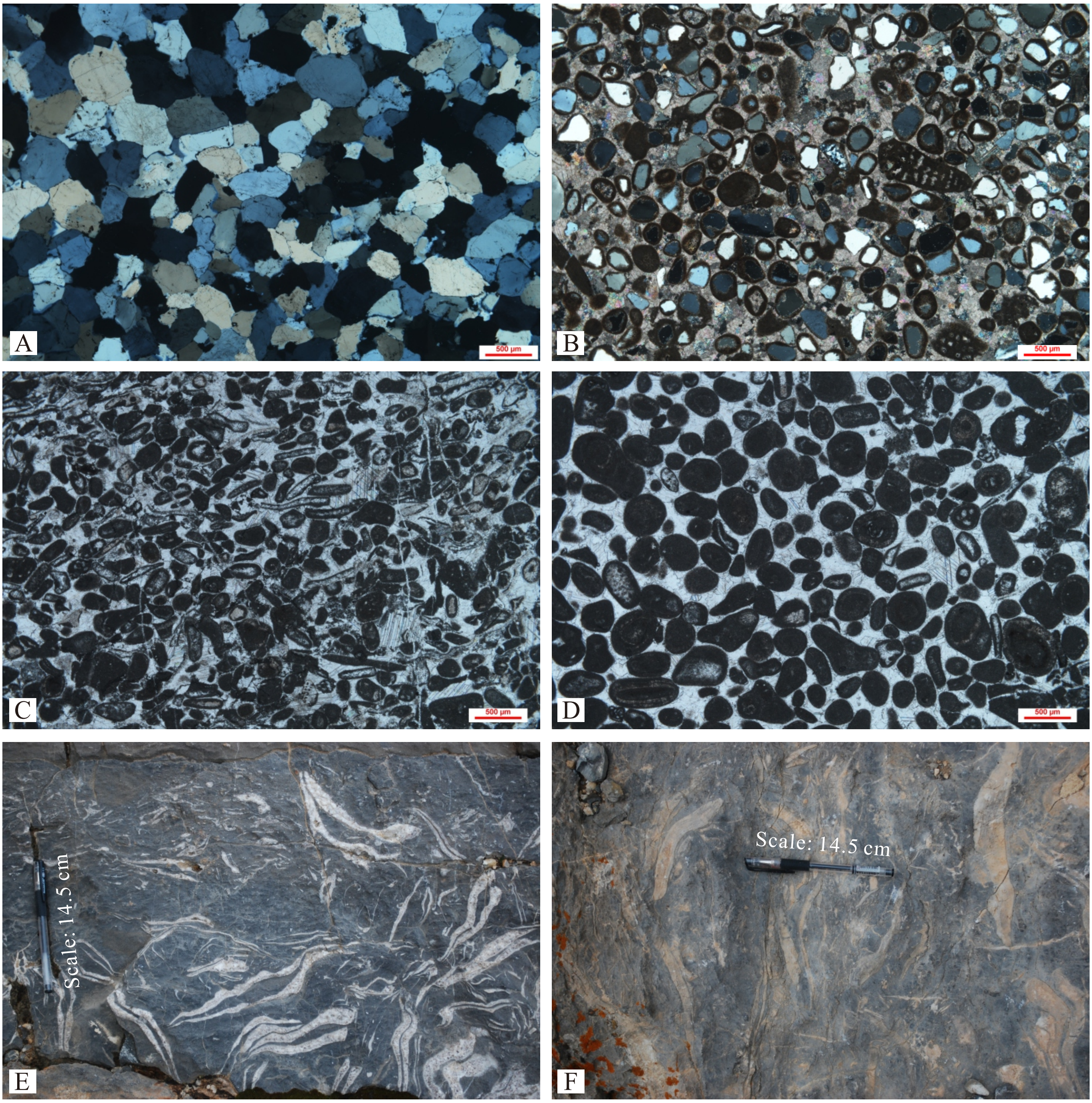

Fig. 9

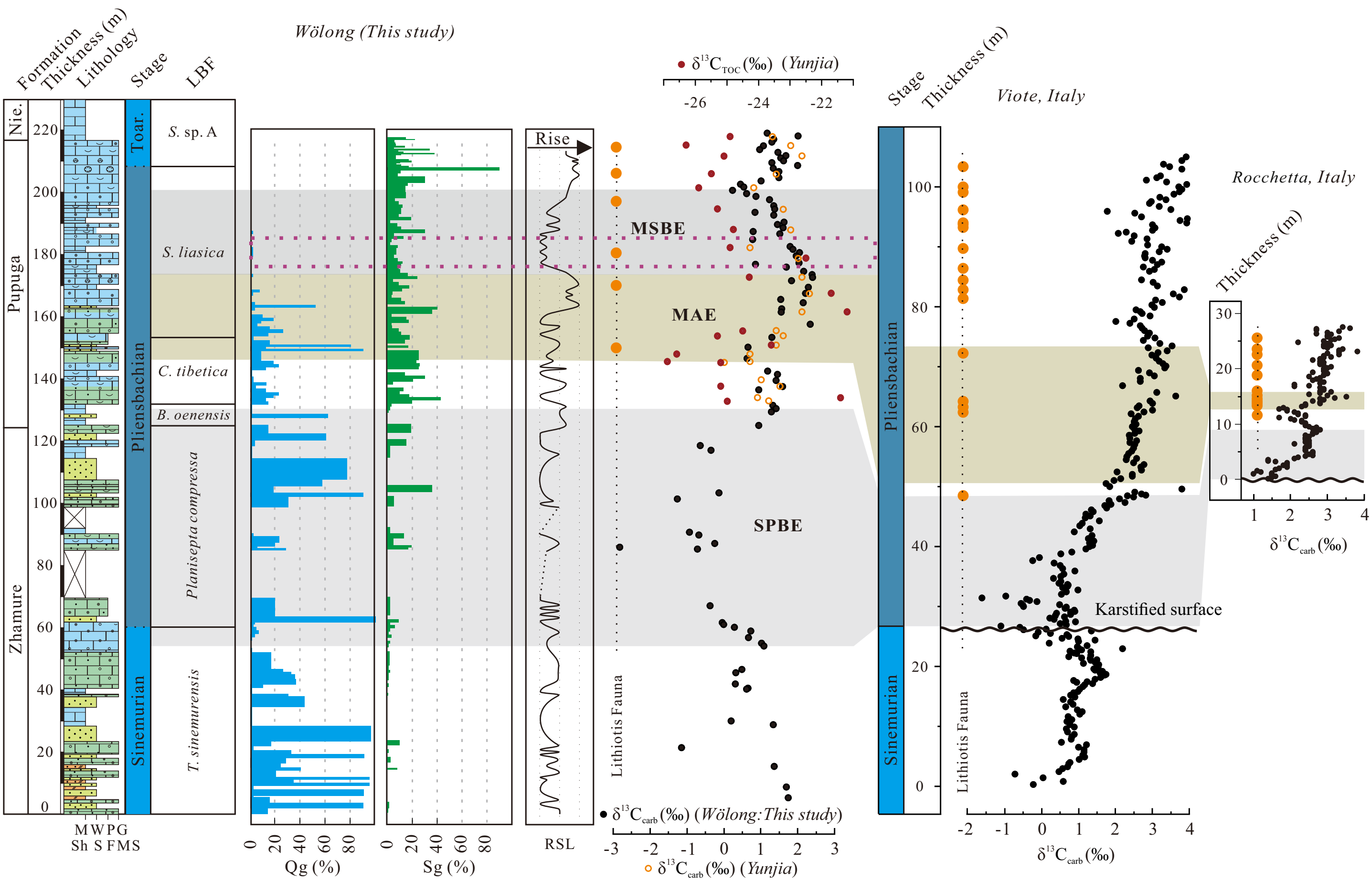

Formation
Thickness (m)
Lithology
Stage
LBF
Wölong (This study)
Nie.
Pupuga
Zhamure
Toar.
Pliensbachian
Sinemurian
S. sp. A
S. liasica
C. tibetica
B. oenensis
Planisepta compressa
T. sinemurensis
M W P G
Sh S F M S
Qg (%)
Sg (%)
Rise
RSL
MSBE
MAE
SPBE
Lithiotis Fauna
δ13C_TOC (‰) (Yunjia)
δ13C_carb (‰) (Wölong: This study)
δ13C_carb (‰) (Yunjia)
Stage
Thickness (m)
Viote, Italy
Karstified surface
δ13C_carb (‰)
Rocchetta, Italy
Thickness (m)
δ13C_carb (‰)